SANDIA REPORT

SAND2012-8714
Unlimited Release
Printed October 2012

Radiant Heating Cookoff Experiments and Predictive Simulations for Fast Cookoff

Marcia A. Cooper
William W. Erikson
Michael S. Oliver
Michael J. Kaneshige
Daniel Sandoval

Prepared by
Sandia National Laboratories
Albuquerque, New Mexico 87185 and Livermore, California 94550

Sandia National Laboratories is a multi-program laboratory managed and operated by Sandia Corporation, a wholly owned subsidiary of Lockheed Martin Corporation, for the U.S. Department of Energy's National Nuclear Security Administration under contract DE-AC04-94AL85000.

Approved for public release; further dissemination unlimited.

Sandia National Laboratories

Issued by Sandia National Laboratories, operated for the United States Department of Energy by Sandia Corporation.

NOTICE: This report was prepared as an account of work sponsored by an agency of the United States Government. Neither the United States Government, nor any agency thereof, nor any of their employees, nor any of their contractors, subcontractors, or their employees, make any warranty, express or implied, or assume any legal liability or responsibility for the accuracy, completeness, or usefulness of any information, apparatus, product, or process disclosed, or represent that its use would not infringe privately owned rights. Reference herein to any specific commercial product, process, or service by trade name, trademark, manufacturer, or otherwise, does not necessarily constitute or imply its endorsement, recommendation, or favoring by the United States Government, any agency thereof, or any of their contractors or subcontractors. The views and opinions expressed herein do not necessarily state or reflect those of the United States Government, any agency thereof, or any of their contractors.

Printed in the United States of America. This report has been reproduced directly from the best available copy.

Available to DOE and DOE contractors from
U.S. Department of Energy
Office of Scientific and Technical Information
P.O. Box 62
Oak Ridge, TN 37831

Telephone: (865) 576-8401
Facsimile: (865) 576-5728
E-Mail: reports@adonis.osti.gov
Online ordering: http://www.osti.gov/bridge

Available to the public from
U.S. Department of Commerce
National Technical Information Service
5285 Port Royal Rd
Springfield, VA 22161

Telephone: (800) 553-6847
Facsimile: (703) 605-6900
E-Mail: orders@ntis.fedworld.gov
Online ordering: http://www.ntis.gov/help/ordermethods.asp?loc=7-4-0#online

SAND2012-8714
Unlimited Release
Printed October 2012

Radiant Heating Cookoff Experiments and Predictive Simulations for Fast Cookoff

Marcia A. Cooper
William W. Erikson
Michael S. Oliver
Michael J. Kaneshige
Daniel Sandoval

Sandia National Laboratories
P.O. Box 5800, MS 1454
Albuquerque, NM 87185-1454
macoope@sandia.gov

Abstract

Thermal initiation (cookoff) of energetic material-laden devices (rocket motors and munitions) during accidental fires is an important safety concern. An article within a pool fire is an example of potential fast cookoff scenerio that has significant potential for a catastrophic result. Beginning in 2007, a collaborative experimental and model development research program under the Joint Munitions Program (JMP) was initiated at SNL/NM to address energetic material response to fast cookoff. The efforts expanded our ongoing research program studying slow cookoff phenomena and sought to answer the key question of "Can our kinetics models derived under slow cookoff conditions be applied to accurately represent energetic material behavior at fast cookoff conditions?" The simplest categorization of slow cookoff is material centered within the energetic material whereas a fast cookoff event is material ignition that occurs at a heated boundary. The external heating rate related to the heat conduction within the energetic material determines the ignition location and thus, the cookoff charaterization of slow or fast. We have developed a benchtop experiment that confines an energetic material sample and exposes it to constant incident heat fluxes common in fire in a controlled and reproducible fashion. Temperatures within the sample near the heated surface are measured using thermocouples and the time-to-event is determined

as a function of incident heat flux. Insight and guidance into the experimental development has been provided by one- and three-dimensional simulations of the heat flow paths through the device. Coupling a chemical kinetics model with the heat transfer calculations enable computational predictions of time-to-ignition for comparison to the experimental data. Experimental and predicted data for PBXN-109, PBX-9501, PBX-9502, and Composition B are presented. The final section of this report presents an initial approach aimed at studing the effect of confinement on ignition and sustained reaction.

Contents

List of Figures 6
1 Introduction 7
2 Experimental Description 8
2.1 Confinement Vessel 9
2.2 Incident Heat Flux 9
3 Model Development Activities 11
4 Energetic Material Comparisons 14
5 Conclusions 16
References 17
6 Appendix A 19
7 Appendix B 32
8 Appendix C 47

Figures

1 Illustration of Radiant Heat Apparatus. 8

2 Illustration of TC arrangement in EM (left) and section view of current confinement design (right). 9

3 Cutaway of the finite element mesh of the radiant heat apparatus. Left: full model with lamp filaments, box and confinement materials. Right: Detail emphasizing interface between aluminum cover plate and EMa very fine mesh was used to capture the steep temperature gradient occurring just under the EM surface. The finest mesh gradation was 13 μm. 11

4 Time to ignition data for PBXN-109 with the Radiant Heating FCO apparatus. Also shown are lines representing the full 3-D model (dashed line) as well as a 1-D model (solid lines) in which the surface heat flux was adjusted to account for non-uniformities and losses down the bolts. (See Appendix B) 12

5 Time-to-event data (left) and temperature at rupture (right) for PBXN-109, PBX-9501, and Composition B. 14

6 Temperature histories measured from a test with PBX 9501 (left) and Composition B (right). 15

7 Comparison of Experiment and Model for Composition B and PBX-9501 15

1 Introduction

Understanding energetic material (EM) response when subjected to rapid heating on the order of 10-1000°C/sec is important when predicting the hazards associated with fast cookoff scenarios. Ongoing research at Sandia National Laboratories using the Sandia Instrumented Thermal Ignition apparatus has enhanced our thermochemical prediction capabilities and understanding of material response at relatively slow heating rates. This research is aimed at determining whether the rates associated with the chemical and physical processes that occur for cases of slow cookoff can merely be extrapolated to cases of fast cookoff.

The hazards associated with a munition in an abnormal thermal environment motivate an understanding of the preignition energetic material behavior and the resulting post-ignition violence. Extensive prior experimental and computational work has been conducted studying slow heating rates ($\approx$10°C/min) on confined explosives [11]. For these cases, in situ thermocouples have been used successfully to observe the preignition material behavior enabling the development of reduced chemical kinetic models and phase-change parameters for HMX [8], RDX [9], PBX-9501 and PBXN-109 [10], and Bullseye [3]. Knowledge of realistic hazard scenarios such as crosswind pool fires suggests that munitions will experience significantly greater rates of temperature increase than what is being studied in the case of slow cookoff. Heat fluxes between 40 and 400 kW/m^2 have been measured on test articles in crosswind pool fires [12, 13, 7, 6]. Such hazardous environments have motivated several policy statements related to fast cookoff. In particular, STANAG 4240 titled "Liquid Fuel Fire, Tests for Munitions" states specific criteria for the testing methodology and evaluation criteria. To address this real-world hazard on a laboratory scale, we seek to develop a fast-cookoff test bed that will allow accurate prediction of full-scale behaviors via approximate correlations, scaling relations, and/or computational modeling. To correlate the small-scale results to large-scale events, the appropriate boundary conditions must be applied, the energetic material response must be similar to the large test, and system behavior (i.e. coupling between the energetic material and confinement) must represent the large-scale.

Our work studing the response of an energetic material to fast cookoff has progressed from a simple arrangement with unconfined explosives and a heated plunger to include full explosive confinement and internal temperature measurements. Details of our earliest efforts with heated plungers is not repeated here but is included in a previous JANNAF article by Cooper et al. [1] in Appendix A. To better represent the real-world hazard of a munition heated in a crosswind pool fire, a radiant-heat test bed has been developed for non-contact heating of a confined explosive pellet. This device has undergone several design iterations which are discussed in more detail within a previous JANNAF article by Erikson et al. [4] in Appendix B. The purpose of this report is to provide construction details of the final version of the experiment along with the experimental data and model predicitions.

2 Experimental Description

Throughout our program studying fast cookoff, we have aimed to meet four main objectives with the experimental apparatus:

1. **Sub-scale EM samples**. Tests are conducted with cylindrical EM samples 2.54-cm in diameter. The samples will be exposed to the radiant heat flux from one of the flat faces establishing a one-dimensional thermal gradient through the sample.

2. **Sufficient range of incident heat fluxes**. Heat fluxes will span the range of 40 to 400 kW/m^2; consistent with a fire environment.

3. **Internal diagnostics**. Temperatures inside the EM itself will be monitored during the tests.

4. **Experiment is controllable and reproducible**.

Throughout the experimental development, from the unconfined heated plunger tests through to the final version of the radiant heat apparatus with confinement, these goals have been met. The rest of this document will present the design details and experimental and model predictions from the final version of the Radiant Heating Apparatus.

A cutaway view of the final version of the radiant-heat apparatus appears in Fig. 1. The apparatus consists of the confined explosive pellet, base plate, lamp assembly, and membrane position detector. Below the EM an o-ring prevents gas leakage outside the support piston. The thermocouple probes, which pass through the piston, also have a gas-tight fit; they are sealed with epoxy bonded to the bottom of the piston support.

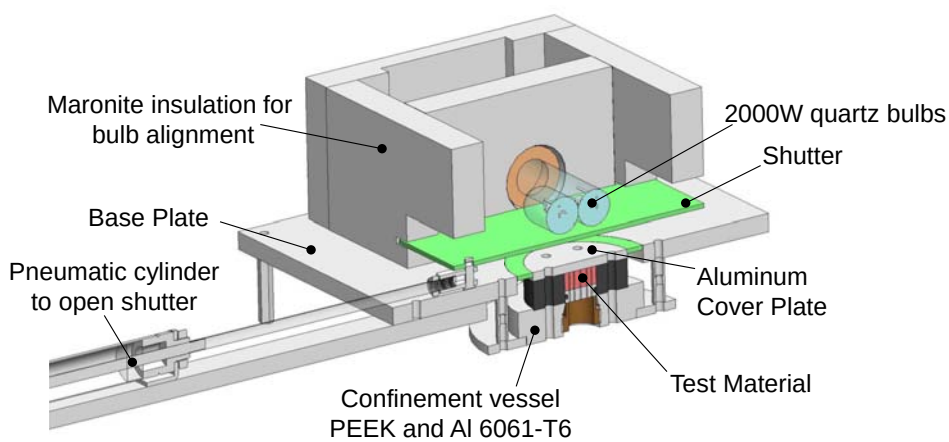

Figure 1. Illustration of Radiant Heat Apparatus.

2.1 Confinement Vessel

The most recent design is one that ensures one-dimensional heating, no/minimal cover plate deformation, known boundary conditions, and a hermetic seal will be maintained on the EM sample until after ignition occurs. This is accomplished by a two-part aluminum and PEEK (Quadrant EPP Ketron® PEEK 1000) surround that is sealed with a 6.35 mm thick, 7.62-cm-diameter aluminum cover plate painted with high emissivity Pyromark®. A ring-shaped knife edge is machined into the cover plate. As the bolts are tightened, the knife edge digs into the upper surface of the PEEK to provide a gas-tight seal on the upper face. Below the EM, an o-ring prevents gas leakage outside the support piston. The thermocouple probes, which pass through the piston, also have a gas-tight fit; they are sealed with epoxy bonded to the bottom of the piston support. Figure 2 shows the embedded TC position and depth arrangement and a cutaway view of the confinement vessel. The pedestal is used to fix the pellet support and EM pellet within the casing forming the confinement vessel. Engineering drawings of these major components of the confinement vessel are given in Appendix C.

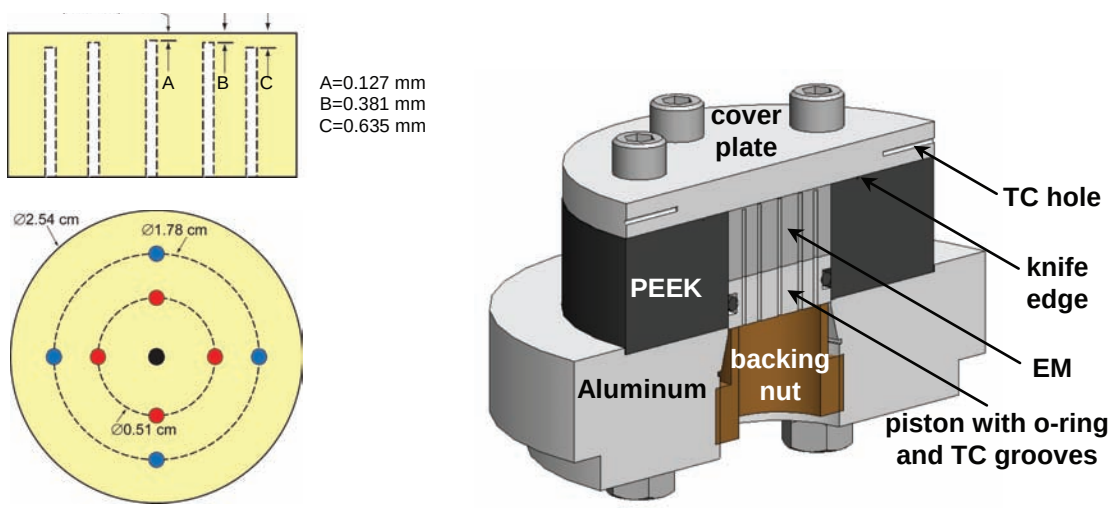

Figure 2. Illustration of TC arrangement in EM (left) and section view of current confinement design (right).

2.2 Incident Heat Flux

Radiant energy incident on the confined explosive pellet is generated by quartz lamps with tungsten filaments. Two 2000 W quartz lamps (ANSI Type BWF) were used to produce the desired range of heat fluxes. They were held in place within a Marinite® (calcium silicate/inert fillers) box to provide structural support that can withstand high temperatures without smoldering. The lamps were aligned horizontally so that the tungsten filaments were directly above the EM. The box structure was placed on top of an aluminum floor into which

a center hole had been cut to allow the introduction of the EM and confining materials as shown in Fig. 1. A pneumatically operated shutter made of Marinite® is located between the bulbs and the test sample. This allows the bulbs to warm up to the desired power level prior to exposing the lower structure.

Prior to each test, a heat flux gauge (Vatell Thermogage circular foil heat transducer) having the same 2.54 cm diameter size as the EM samples, was placed in the holding fixture. The surface of that gauge was painted with the same surface finish (high emissivity black coating) as the EM sample cover plates would be. Heat flux measurements were made as a function of the current supplied to each lamp. Current was controlled with an Omega Phase Angle Fired SCR power controller (Appendix A). The lamps have an overall length of 19.05 cm (7.5 in) and each bulb has a diameter of 2.54 cm (1 in) with a type CC-8 tungsten filament. Omega phase-delay relays are used to control power to the lamps based on a 0-10 VDC control voltage. At full operation, each bulb requires approximately 16 amps at 120 VAC. The heat flux gauge gives a single reading which averages the response of the entire 2.54 cm diameter sensing surface. A variation of 11% was measured and predicted across the cover plate surface (Appendix A).

3 Model Development Activities

Owing to the one-dimensional behavior of the experimental apparatus, simulations were able to proceed in a fully predictive, three-dimensional arrangement or in a one-dimensional methodology that uses the measured boundary conditions to represent the EM behavior.

The three-dimensional simulations were made to predict the behavior of the design using finite element models illustrated in Fig. 3. The simulations showed that there was nearly one-dimensional heat transfer in the vertical direction since the aluminum has high thermal conductivity enabling the thick cover plate is able to smooth out variations in temperature resulting from uneven radiant heating. In addition, since PEEK and the EM are both fairly good insulators (≈0.25 W/m-K for PEEK, ≈0.6 W/m-K for PBXN-109), there was no dominant path for heat conduction either to the outside (i.e. through the PEEK) or to the inside (through the EM). The combination of these two effects resulted in a nearly one-dimensional (vertical direction) flow of energy through the EM. There were concerns that the six steel bolts which hold the apparatus together would be preferential heat conduction paths and produce complex temperature profiles. To analyze their effects, the bolts were included in the finite element model. Though some multi-dimensional effects associated with the bolts were evident, simulations indicated that heat transfer along the bolts did not appear to adversely affect the temperature profiles within the EM itself (i.e. no obvious change in temperature pattern was observed in the EM).

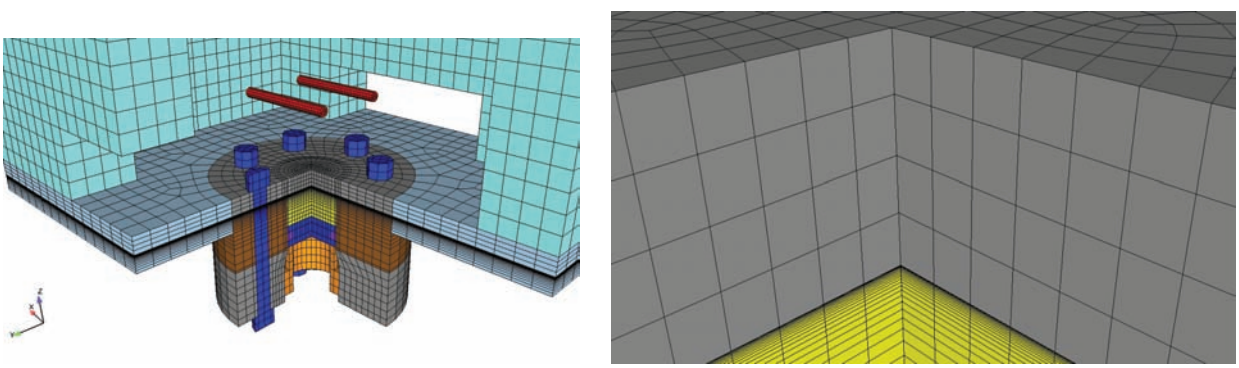

Figure 3. Cutaway of the finite element mesh of the radiant heat apparatus. Left: full model with lamp filaments, box and confinement materials. Right: Detail emphasizing interface between aluminum cover plate and EMa very fine mesh was used to capture the steep temperature gradient occurring just under the EM surface. The finest mesh gradation was 13 μm.

The one-dimensional geometry has some advantages in that it can be meshed more finely (appropriate for the fast heating where gradients are strong and ignition is expected near the interface between EM and confinement materials) and still remain a tractable problem.

The one-dimensional model included three layers: a 6.35 mm thick aluminum layer, a 12.7 mm thick EM layer, and an 8.64 mm thick layer representing the support piston. The mesh spacing was 1 μm in the region near the aluminum-EM interface. Chemical reaction mechanism from the literature were used to describe the decomposition leading to ignition.

In the one-dimensional geometry, two approaches can be used for the hot boundary condition. The first approach is to use a heat flux boundary condition. However, as described above (and in more detail in Appendix B), because of non-uniform flux distribution and preferential paths, it is not clear what heat flux value to use for that boundary condition. We have been successful at adjusting the heat flux to account for these non-uniformities and reproducing the behavior. An example of this is illustrated in Fig. 4 for PBXN-109 which utilized a decomposition model derived from slow cookoff data [5]. The 3-D model which accounts for the details of the complex heat transfer paths gives results which represent the data quite well. The 1-D model can also represent the data, but this required the incident heat flux to be adjusted by dividing the measured heat flux by 0.65 to account for the non-uniformity of the flux on the surface and also accounting for the 10 to 20% heat loss down the bolts (two lines are plotted in Fig. 4, one with 10% bolt heat loss, the other with 20% bolt heat loss). See Appendix B for a more thorough explanation of the corrections and how these were determined.

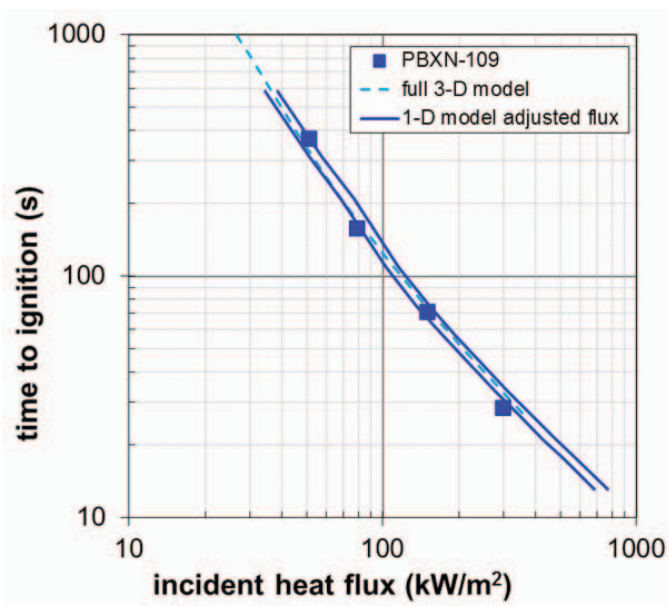

Figure 4. Time to ignition data for PBXN-109 with the Radiant Heating FCO apparatus. Also shown are lines representing the full 3-D model (dashed line) as well as a 1-D model (solid lines) in which the surface heat flux was adjusted to account for non-uniformities and losses down the bolts. (See Appendix B)

It has been demonstrated that one can represent the device with a 1-D model with a heat flux boundary condition. But because this requires the heat flux corrections described above, it is not entirely satisfying. Fortunately a second method is available and is discussed with the experimental data from PBX-9501 and Composition B in the next section.

4 Energetic Material Comparisons

To date, PBXN-109, PBX-9501 and Composition B have been tested in the radiant heat apparatus to assess its time-to-event behavior as a function of heat flux. The data is given in Fig. 5.

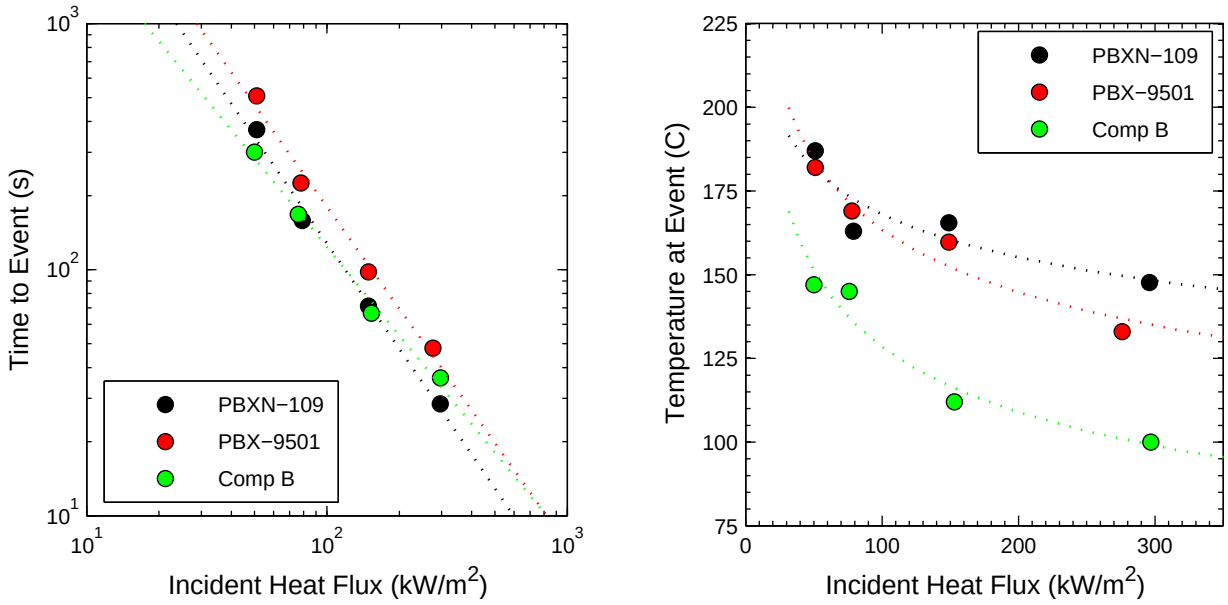

Figure 5. Time-to-event data (left) and temperature at rupture (right) for PBXN-109, PBX-9501, and Composition B.

The second modeling approach is to use the same finely meshed 1-D model but instead apply a time-varying temperature boundary condition which corresponds to the temperature data from the thermocouples located within the aluminum cover plate (Fig. 6). That is, to use experimental data to automatically correct for non-uniformities. Example results from the second approach are given in Fig. 7 which shows time to ignition data for Composition B and PBX 9501. Also shown in Fig. 7 are results from a 1-D geometric model with various decomposition heat release models. For Composition B, the Prout-Tompkins form given by Wemhoff and Burnham [14] was used. For PBX 9501, two models were used: the Dickson et al. [2] model and a model published by Hobbs et al. [8]. Note that all three of these models represent the FCO data quite well.

It should be noted that while this second approach to the 1-D modeling is very effective (all of the models represented their respective data well), it is not predictive. That is, the time-temperature histories to be used as the surface boundary condition are not known a priori. Nevertheless, the goal to demonstrate that models derived from slow cookoff data are able to represent time to ignition at very high heating rates seems to have been accomplished.

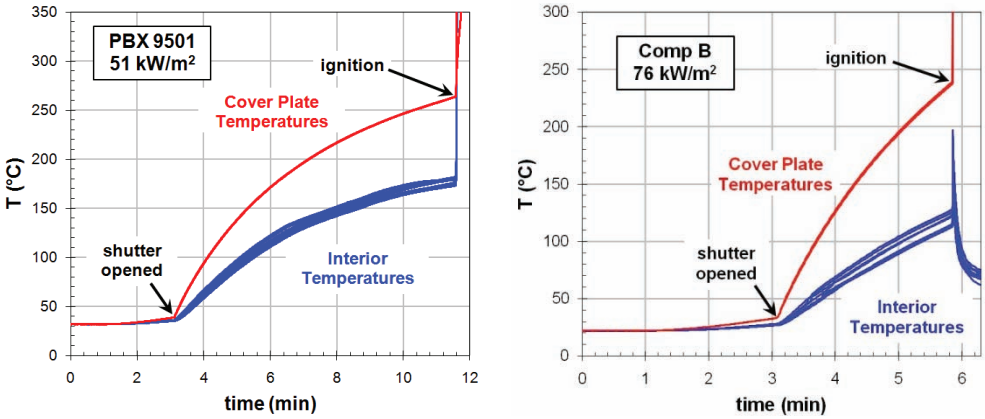

Figure 6. Temperature histories measured from a test with PBX 9501 (left) and Composition B (right).

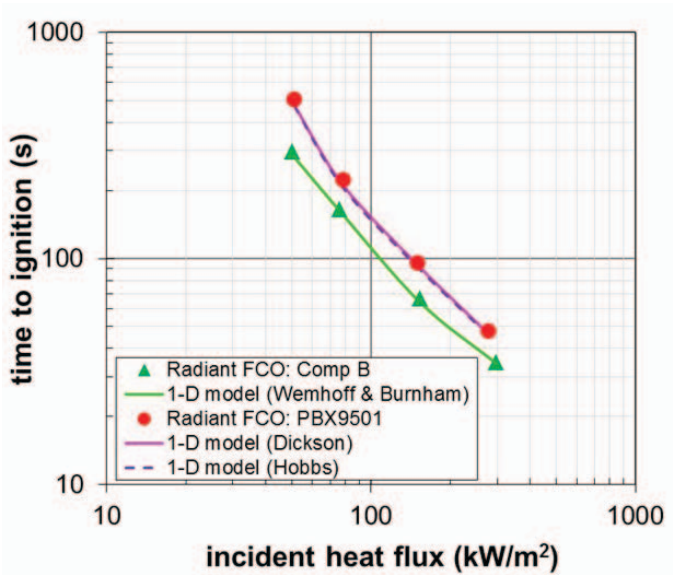

Figure 7. Comparison of Experiment and Model for Composition B and PBX-9501

5 Conclusions

A collaborative expermental and model development program studing EM response to fast cookoff has established a basis for the continued application of slow-cookoff derived chemistry models to be applied to the situation of fast cookoff. Through the experimental and simulation of three EM materials, it has been demonstrated that the experimental data can be sufficiently predicted using these slow cookoff models. These results were verified with our final Radiant Heat apparatus deesign that confines an EM pellet and applies an external heat flux in one dimension.

One- and three-dimensional simulations of the experimental setups were created. Thermal models were able to capture the spatial heat flux distribution produced by the radiant heating lamps. The models were also able to represent well the time to ignition for PBXN-109, PBX-9501 and Composition B. For this final Radiant Heat apparatus, 3-D modeling results were true predictions, performed prior to the experiments being conducted and captured well the time to ignition. It could also be modeled with a 1-D model, but it was necessary to make some corrections to the imposed heat flux to account for non-uniformities and bolt heat losses which had been represented in the 3-D model.

References

[1] M. A. Cooper, W. W. Erikson, D. Sandoval, and M. J. Kaneshige. Development of a fast cookoff test bed at sandia national laboratories. In *Joint Army-NASA-Air Force (JANNAF) 24th Propulsion Systems Hazards Subcommittee Meeting*, Newton, MA, 2008. May 12-16. SAND2008-2951C.

[2] P. M. Dickson, B. W. Asay, B. F. Henson, C. S. Fugard, and J. Wong. Measurement of Phase Change and Thermal Decomposition Kinetics During Cookoff of PBX 9501. *AIP Conference Proceedings*, 505(1):837–840, 2000.

[3] A. B. Dodd and M. J. Kaneshige. Cook-Off Model Development and Analysis of Energetic Materials Using Sandia Instrumented Thermal Ignition (SITI) Experimental Data. In *13th International Detonation Symposium*, Norfolk, VA, 2006. July 23-28.

[4] W. W. Erikson, M. A. Cooper, and M. S. Oliver. Radiant heating cookoff experiments and associated models. In *Joint Army-NASA-Air Force (JANNAF) 25th Propulsion Systems Hazards Subcommittee Meeting*, La Jolla, CA, 2009. December 7-11. SAND2009-7893C.

[5] W. W. Erikson and R. G. Schmitt. Modeling Thermal Decomposition and Deflagration in Small- and Munition-Scale Navy Cookoff Experiments. In *Joint Army-NASA-Air Force (JANNAF) 21st Propulsion Systems Hazards Subcommittee Meeting*, Colorado Springs, CO, 2003. December 1-5.

[6] J. J. Gregory, R. Mata Jr., and N. R. Keltner. Thermal Measurements in a Series of Large Pool Fires. Technical Report SAND85-0196, Sandia National Laboratories, Albuquerque, New Mexico, August 1985.

[7] L. A. Gritzo and V. F. Nicolette. Coupling of Large Fire Phenomenon with Object Geometry and Object Thermal Response. Technical Report SAND97-1364, Sandia National Laboratories, Albuquerque, New Mexico, 1997.

[8] M. L. Hobbs and M. J. Kaneshige. Modeling HMX Ignition Using an Enthalpy Formulation. In *13th International Detonation Symposium*, Norfolk, VA, 2006. July 23-28.

[9] M. L. Hobbs, M. Steyskal, and M. J. Kaneshige. Modeling RDX Ignition. In *Joint Army-NASA-Air Force (JANNAF) 24th Propulsion Systems Hazards Subcommittee Meeting*, Newton, MA, 2008. May 12-16.

[10] M. J. Kaneshige, A. M. Renlund, R. G. Schmitt, and W. W. Erikson. Cook-Off Experiments for Model Validation at Sandia National Laboratories. In *12th International Detonation Symposium*, San Diego, CA, 2002. August 11-16.

[11] M. J. Kaneshige, A. M. Renlund, R. G. Schmitt, and W. W. Erikson. Improvements in Cook-Off Models Using Real-Time In Situ Measurement of Temperature and Pressure. In *Joint Army-NASA-Air Force (JANNAF) 21st Propulsion Systems Hazards Subcommittee Meeting*, Colorado Springs, CO, 2003. December 1-5.

[12] M. A. Kramer, M. Greiner, and J. A. Koski. Radiation Heat Transfer to the Leeward Side of a Massive Object Suspended over a Pool Fire. In *International Mechanical Engineering Congress and Exposition*, New York, NY, 2001. November 11-16.

[13] J. M. Suo-Anttila and L. A. Gritzo. Thermal Measurements from a Series of Tests with a Large Cylindrical Calorimeter on the Leeward Edge of a JP-8 Pool Fire in Cross-Flow. Technical Report SAND2001-1986, Sandia National Laboratories, Albuquerque, New Mexico, July 2001.

[14] A. P. Wemhoff and A. K. Burnham. Prout-Tompkins Decomposition Kinetics Formulation. In C. Owens, editor, *LLNL Explosives Reference Guide*, chapter 6. LLNL, 4 2010. LLNL-WEB-436051.

6 Appendix A

M. A. Cooper, W. W. Erikson, D. Sandoval, and M. J. Kaneshige, "Development of a Fast-Cookoff Test Bed at Sandia National Laboratories", JANNAF 42rd CS, 30st APS and 24th PSHS Joint Meeting, Boston, MA. May 2008. Unlimited Release, SAND2008-2951C

Development of a Fast-Cookoff Test Bed at Sandia National Laboratories

Marcia A. Cooper, William W. Erikson, Daniel Sandoval, and Michael J. Kaneshige*
Sandia National Laboratories
Albuquerque, New Mexico, 87185

ABSTRACT

Understanding energetic material response when subjected to rapid heating on the order of 10-1000°C/sec is important when predicting the hazards associated with fast cookoff scenarios. Ongoing research at Sandia National Laboratories using the Sandia Instrumented Thermal Ignition apparatus has enhanced our thermochemical prediction capabilities and understanding of material response at relatively slow heating rates. It is currently unknown whether the rates associated with the chemical and physical processes that occur for cases of slow cookoff can merely be extrapolated to cases of fast cookoff.

Development of a fast-cookoff test bed is ongoing. Work has progressed from a simple arrangement with unconfined explosives and a heated plunger to include full explosive confinement and internal temperature measurements. Explosive confinement may lead to relatively benign events such as a small rupture of the vessel followed by quenching of the chemical reactions to relatively violent events such as complete and rapid fragmentation of the vessel. Experimental challenges associated with the heated-plunger test bed include the finite thermal mass of the plunger and variations in contact resistance at the plunger-confinement vessel interface. To better represent the real-world case of non-contact heating from a large pool fire and to avoid the experimental challenges associated with the heated plunger, a radiant-heat test bed has been developed. Materials of current interest include PBX-9501, PBXN-109, and Composition B. A summary of the test bed development and representative experimental and computational results are presented.

I. INTRODUCTION

The hazards associated with a munition in an abnormal thermal environment motivate an understanding of the preignition energetic material behavior and the resulting post-ignition violence. Extensive prior experimental and computational work has been conducted studying slow heating rates ($\sim$10°C/min) on confined explosives [1]. For these cases, in situ thermocouples have been used successfully to observe the preignition material behavior enabling the development of reduced chemical kinetic models and phase-change parameters for HMX [2], RDX [3], PBX-9501 and PBXN-109 [4], and Bullseye [5].

Knowledge of realistic hazard scenarios such as crosswind pool fires suggests that munitions will experience significantly greater rates of temperature increase than what is being studied in the case of slow cookoff. Heat fluxes between 40 and 400 kW/m^2 have been measured on test articles in crosswind pool fires [6–9]. Such hazardous environments have motivated several policy statements related to fast cookoff. In particular, STANAG 4240 titled "Liquid Fuel Fire, Tests for Munitions" states that a munition must not go propulsive, must not experience a reaction greater than Type V (pressure burst) during the first 5 minutes, and must not experience a reaction greater than Type IV (burning). Current standards for qualification include a full-scale system fully engulfed in a wood or liquid fuel fire where cookoff occurs within 10 minutes and the resulting fragments are used to determine the hazard classification. To address this real-world hazard on a laboratory scale, we seek to develop a fast-cookoff test bed that will allow accurate prediction of full-scale behaviors via approximate correlations, scaling relations, and/or computational modeling. To correlate the small-scale results to large-scale events, the appropriate boundary conditions must be applied, the energetic material response must be similar to the large test, and system behavior (i.e. coupling between the energetic material and confinement) must represent the large-scale.

---

*SAND2008-2951C. Approved for public release; distribution is unlimited.

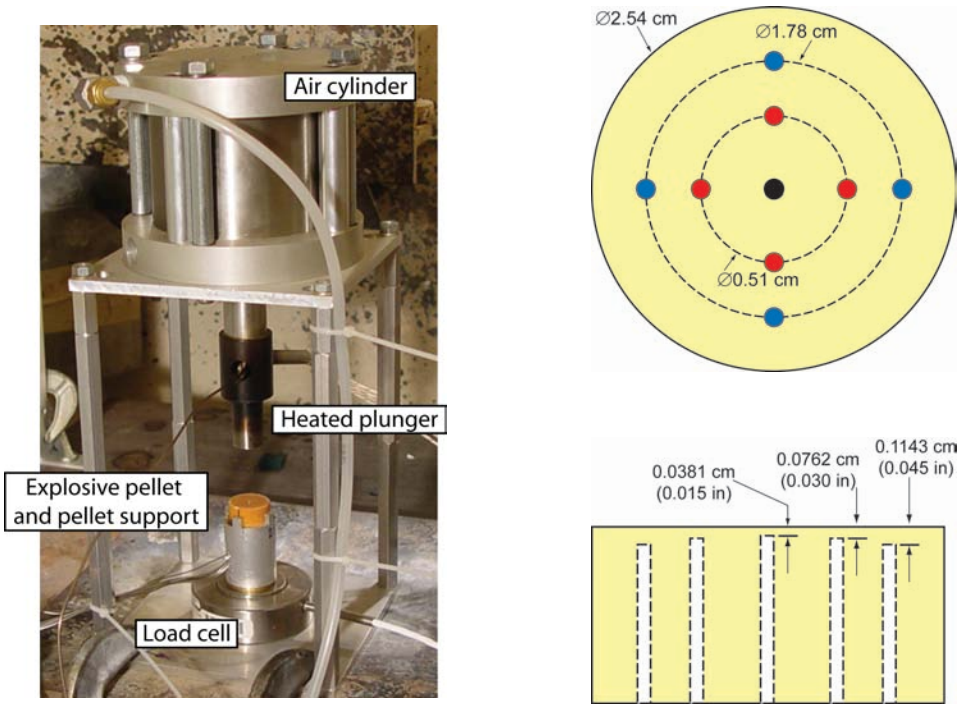

FIG. 1: Photograph of heated-plunger test bed with 2.54-cm-diameter plunger and unconfined explosive pellet on left. Illustration of thermocouple locations on right.

The following sections describe our development efforts with a heated-plunger test bed using unconfined explosive pellets (Section II) and confined explosive pellets (Sections III). Thermochemical modeling results for the heated-plunger test bed appear in Section IV. The radiant-heat test bed and initial results are presented in Section V.

II. HEATED-PLUNGER TEST BED WITH UNCONFINED EXPLOSIVE PELLETS

The first phase of test bed development used a heated plunger contacting unconfined explosive pellets. A photograph of the test bed with an unconfined pellet appears in the left side of Fig. 1. The plunger was initially heated and then brought into contact with the explosive pellet. The effect of plunger temperature on the time-to- and type-of-event was measured.

EXPERIMENT DETAILS

A stainless steel plunger with a 1.91-cm (0.75-in) diameter and 3.81-cm (1.5-in) length was heated with three 50-W cartridge heaters (Omega CSS-10150/120V) to an initial temperature between 300-600°C. Heater power was controlled by a sheathed K-type thermocouple (KTSS Series from Omega) with a diameter of 1.6 mm (1/16 in) that was installed along the plunger centerline at the contact surface. A single-acting air cylinder (FOS Series from Bimba Manufacturing) was used to lower the heated plunger into contact with the explosive pellet. The explosive pellet had a diameter of 2.54 cm (1 in) and height of 1.27 cm (0.5 in). Vertical alignment of the fully-extended plunger and the explosive pellet was conducted prior to heating by locating the pellet under the plunger such that the supporting load cell (Sensotec Model D) detected a force of 50-200 lbf. By aligning the pellet to the fully-extended plunger, no additional downward movement of the plunger occurred during a test to maintain contact if the explosive surface receded due to melting or material loss.

Nine thermocouples were distributed over the cross-sectional area of the pellet and embedded at varying depths from the contact surface. Thermocouple placement is illustrated in the right side of Fig. 1. Blind

TABLE I: Tests conducted with heated plunger and unconfined explosive pellet. Δt corresponds to the time delay in seconds (averaged over all tests at each initial plunger temperature) from contact with the heated plunger until the first observation of gas generation or flame. Numbers in parentheses are the fraction of total tests at each initial plunger temperature in which the observed response was obtained.

Plunger Temp.	PBX-9501		PBXN-109	Composition B
(°C)	Δt (gas)	Δt (flame)	Δt (gas)	
600	0 (1/1)	0.25 (1/1)	0 (1/1)	–
450	0 (1/1)	14.2 (1/1)	0 (1/1)	–
400	0 (3/3)	21 (3/3)	–	–
350	1.5 (3/3)	42 (1/3)	10 (1/1)	–
300	30.5 (1/3)	128.7 (1/3)	22 (3/3)	TNT Melt only
275	–	–	38.5 (2/3)	TNT Melt only

holes were drilled into the pellet from the bottom surface to receive the 0.81-mm (0.032-in) sheathed K-type thermocouples (KMQSS Series from Omega). High speed video, typically 1000 frames per second, was recorded for each test.

RESULTS

Most of the explosive pellets tested were instrumented with thermocouples. In the event that no temperatures were recorded within the explosive pellet, high-speed video was used to observe the material response. Tests in which both video and temperatures were obtained showed a correlation between the time of the observed event (i.e. gas generation, flame, melt) and distinct changes in the material temperature. Summary data consisting of the time-to- and type-of-event are tabulated in Table I for PBX-9501, PBXN-109, and Composition B. The fraction of total tests at each initial plunger temperature in which the observed response was obtained is recorded next to each time. At the lower plunger temperatures (350°C and below), less consistency in the material response was observed. Slight experiment-to-experiment variations in contact between the plunger and explosive pellet likely affected the experimental repeatability for these tests near the temperature threshold for ignition.

Representative results for the Composition B material in terms of the explosive and plunger temperatures are given in Fig. 2 along with a post-test photograph clearly showing evidence of melt. Only melting was observed for plunger temperatures up to 300°C so no further testing was conducted. The colored temperature histories plotted in Fig. 2 correspond to the colored thermocouple locations illustrated in the right side of Fig. 1. The thick black line corresponds to the center thermocouple, the red lines correspond to the thermocouples at a diameter of 0.51 cm and the blue lines correspond to the thermocouples at a diameter of 1.78 cm. The plunger temperature decreases from an initial temperature of 300°C after contact with the explosive at 0 seconds. Meanwhile, the explosive material temperatures increase rapidly until temperature oscillations caused by flow of the melted material appear. The TNT melt is observed as a discontinuity in the temperature histories near 80°C. The plunger is removed at approximately 80 seconds and the material cools.

Representative results for the PBXN-109 material in terms of the explosive and plunger temperatures are given in Fig. 3 along with a post-test photograph clearly showing evidence of reaction. The colored temperature histories plotted in Fig. 3 correspond to the colored thermocouple locations illustrated in the right side of Fig. 1. The plunger temperature decreases from an initial temperature of 300°C to a final temperature of 280°C after contact with the explosive at 0 seconds. During heating, the explosive temperatures measured at the center (black) and inner-diameter (red) thermocouples increase at a faster rate than the temperatures measured at the outer-diameter (blue) thermocouples. At 23.5 seconds, the plunger temperature and material temperature measured by the center thermocouple increase rapidly and a significant increase in the gas generation rate is observed in the recorded video. At 33.5 seconds, the explosive temperatures rapidly increase and exceed the plunger temperature indicating energy release by the explosive. The evidence of early-time gas generation followed by later-time material temperatures in excess of the plunger temperature was observed in all three repeat tests. A flameless reaction front was observed to travel downward through the pellet which produced copious amounts of gaseous reaction products.

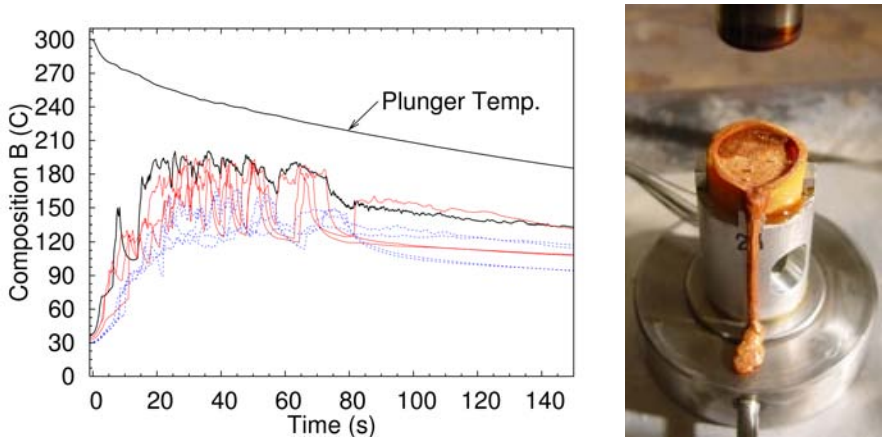

FIG. 2: Plot of explosive and plunger temperatures and photograph of melted Composition B pellet using heated-plunger test bed.

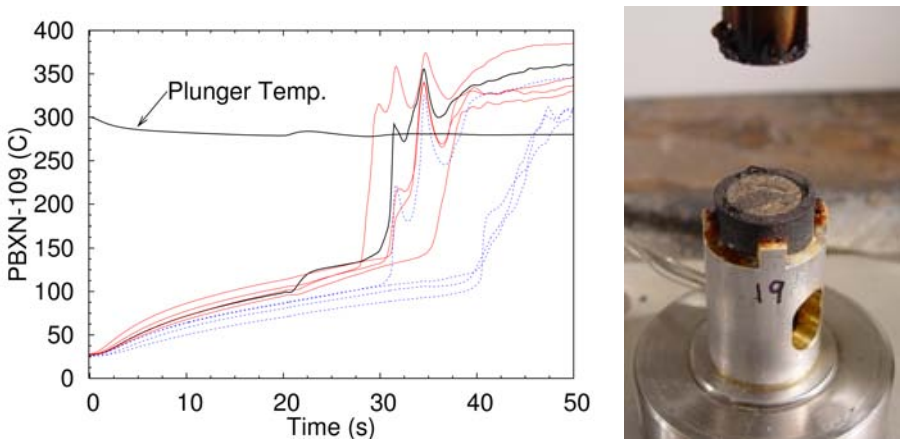

FIG. 3: Plot of explosive and plunger temperatures and photograph of reacted PBXN-109 pellet using heated-plunger test bed.

The time-to-event data of Table I are plotted in Fig. 4 for the events of gas generation for PBXN-109 and of flame generation for PBX-9501. Open symbols indicate that repeat tests did not produce consistent results as indicated in Table I. Solid symbols indicate either a single test was conducted or the results of multiple tests were consistent.

III. HEATED-PLUNGER TEST BED WITH CONFINED EXPLOSIVE

The second phase of test bed development used a heated plunger contacting confined explosive pellets of either PBX-9501 or PBXN-109. An illustration of the test bed with a confined explosive pellet appears in the left side of Fig. 5. The plunger was initially heated and then brought into contact with an aluminum confinement vessel enclosing the explosive pellet. The effect of plunger temperature and plunger type on the time-to- and type-of-event was measured.

EXPERIMENT DETAILS

Initial tests were conducted with a stainless steel plunger with a diameter of 2.54 cm (1 in) and heated with 50-W cartridge heaters. With the addition of heat conduction losses through the confinement vessel,

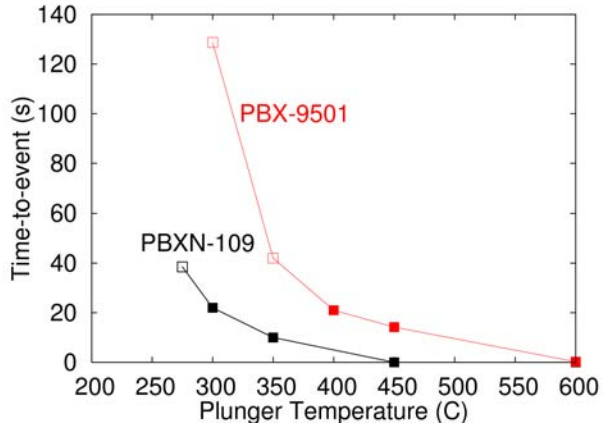

FIG. 4: Comparison of time-to-event data versus initial plunger temperature for PBXN-109 (gas generation) and PBX-9501 (flame).

the plunger temperature was found to decrease significantly during a test. As a result, the plunger was redesigned to have a larger thermal mass which was achieved by increasing its diameter to 10.16 cm (4 in) and constructing it from aluminum. The bottom surface of the plunger necked down to the 2.54-cm (1-in) diameter contact surface as shown in Fig. 5. The larger aluminum plunger was heated with two 550-watt band heaters (Chromalux MBH Series). Heater power was controlled by an embedded thermocouple and the single-acting air cylinder was used to position the plunger onto the confinement vessel as described in Section II.

The aluminum confinement vessel consists of a cylindrical casing and a top ring and bottom plate held together by an array of six bolts. A 0.020-in-thick aluminum membrane was held in place against the top surface of the explosive pellet by the top ring. The plunger contacted this membrane during the test. The membrane sealed against the cylindrical casing for internal pressure using o-rings. The explosive was instrumented with nine thermocouples as in the tests using unconfined pellets. Thermocouple placement is illustrated in the right side of Fig. 5. Vertical alignment with the fully extended plunger and confinement vessel was conducted as before in the unconfined tests. The load cell detected additional axial loads due to pressurization of the confinement vessel during heating. A PolyEtherEtherKetone (PEEK) liner (Ketron® PEEK 1000 manufactured by Quadrant Engineering Plastic Products) was added to the PBXN-109 tests in an effort to inhibit radial heat exchange between the explosive pellet and the cylindrical casing of the vessel.

RESULTS

The confinement vessel contained the product gases generated from the heated explosive until vessel rupture. The aluminum membrane typically ruptured first by partially or completely shearing around the unsupported interface between the outer plunger diameter and the inner diameter of the top ring. Membrane rupture was observed through evidence of sparks or gas jetting on the high-speed video, a rapid decrease in force detected at the load cell, and a rapid decrease in material temperature. Summary time-to-event data appear in Table II where the event corresponds to rupture of the aluminum membrane. In all the confined explosive tests, initial rupture of the aluminum membrane occurred followed by a period of continued explosive heating and a second, more complete, rupture of the vessel in which the bolts no longer held the cylindrical casing firmly between the top clamp ring and bottom plate. The test was terminated after complete rupture of the vessel.

Representative results of the PBX-9501 material in terms of the normalized force (top plot) and explosive and plunger temperatures (bottom plot) are given in Fig. 6. The test was conducted with the stainless steel plunger with a 2.54-cm (1-in) diameter initially heated to 450°C. Evidence of aluminum membrane rupture followed by gas jetting and post-test reacted material was observed. The normalized load cell force increases during the initial heating of the explosive due to gas generation. The force is

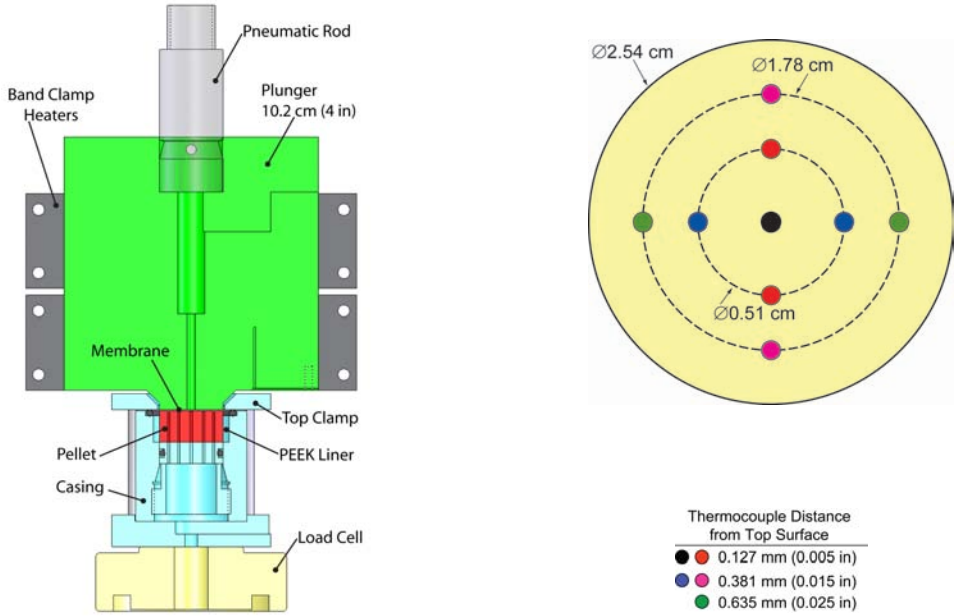

FIG. 5: Photograph of heated-plunger test bed with 10.16-cm-diameter plunger and confined explosive pellet on left. Illustration of thermocouple locations on right.

TABLE II: Tests conducted with heated plunger and confined explosive pellet. Δt corresponds to the time delay in seconds from contact with the heated plunger until the first observation of membrane rupture.

Plunger Temp. (°C)	PBX-9501 Δt (s)	PBXN-109 Δt (s)
500	1.87	–
450	1.14, 1.40	–
325	–	1.4
300	–	33, 42
275	–	123

normalized by the peak load measured just before complete vessel rupture. The colored temperature histories within the explosive correspond to the colored thermocouple locations as illustrated in the right side of Fig. 5. The temperatures are not ordered in terms of their depth from the contact surface as observed in the unconfined tests indicating non-uniform contact resistance between the plunger-aluminum membrane-explosive interfaces and/or potential radial heat transfer losses to the confining vessel. The plunger temperature decreases from 450°C to nearly 375°C during the 7 seconds of test time due to its low thermal mass.

After approximately 0.3 seconds of heating, the thermocouples located in the explosive detect increasing temperature. The temperatures continue increasing until a discontinuity in the force and explosive temperatures is observed at approximately 1.4 seconds. Also at this time, the recorded video shows evidence of aluminum membrane rupture followed by gas jetting. Since the plunger is still in contact with the confinement vessel, continued heating of the explosive enables continued reaction and vessel pressurization. Complete rupture of the vessel occurs at 2.2 sec.

At an initial plunger temperature of 450°C, the aluminum membrane ruptured at 1.13 and 1.40 seconds for two repeat tests. At an initial plunger of 500°C, the aluminum membrane ruptured at 1.87 seconds. The time until membrane rupture is expected to decrease as the plunger temperature increases and this inconsistency is likely affected by undesired radial heat conduction losses into the confinement vessel.

Representative results for the PBXN-109 material in terms of the normalized force (top plot) and explosive and plunger temperatures (bottom plot) are given in Fig. 7. The test was conducted with the 10.16-cm (4-in) diameter aluminum plunger initially heated to 300°C and a PEEK liner separated the explosive-cylindrical casing interface. Evidence of aluminum membrane rupture followed by gas jetting and post-test reacted material was observed. The measured force increases and reaches its

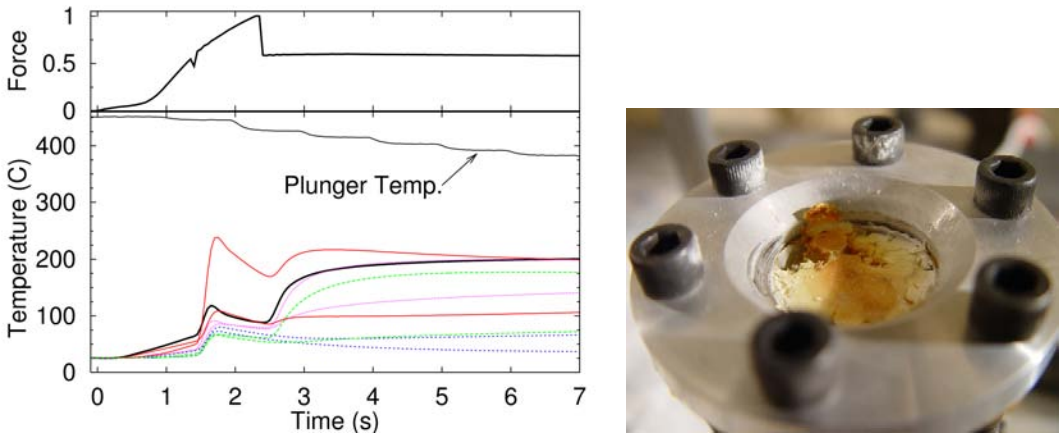

FIG. 6: Plot of explosive and plunger temperatures and normalized force detected at load cell using heated-plunger test bed on left. Post-test photograph of reacted PBX-9501 pellet on right.

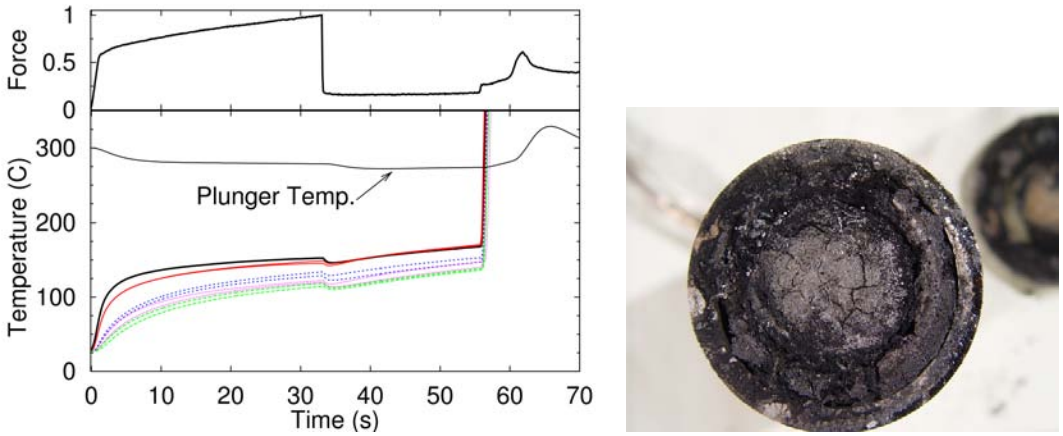

FIG. 7: Plot of explosive and plunger temperatures and normalized force detected at load cell using heated-plunger test bed on left. Post-test photograph of reacted PBXN-109 pellet on right.

peak value immediately before the aluminum membrane ruptures resulting in a time-to-event of 33 seconds. The plunger temperature decreases from 300°C to almost 275°C before vessel rupture illustrating the improvement provided by the larger thermal mass of the plunger. The corresponding explosive temperatures continuously increase during contact with the heated plunger and a discontinuity occurs at the time of vessel rupture. The explosive temperatures are noted to be ordered in terms of depth from the contact surface indicating uniform contact (and heating) by the plunger. After rupture of the aluminum membrane, the plunger becomes seated against the top clamp and a constant force is measured although the explosive continues heating. At approximately 55 seconds, complete rupture of the vessel occurs as noted by rapid venting observed in the video with a corresponding rise in the measured load and evidence of thermal runaway in the measured temperatures.

IV. THERMOCHEMICAL MODELING FOR HEATED-PLUNGER TEST BED

The thermochemical finite element computational code CALORE was utilized as an aid in the preliminary design work of the heated-plunger test bed. The model consists of a 2-D axisymmetric geometry that includes all components of the plunger and confining vessel with realistic material properties, including an energetic chemistry model for PBXN-109 [10]. With the model, specific issues related to the design were explored including: the initial plunger temperature, contact resistance between the plunger

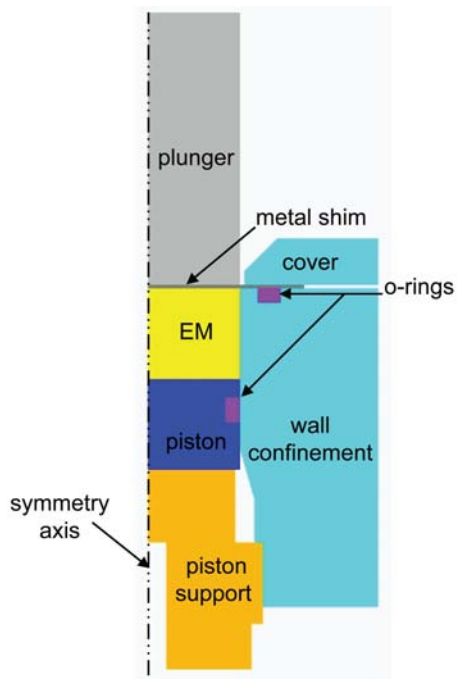

FIG. 8: Thermochemical model geometry illustrating 2.54-cm-diameter plunger.

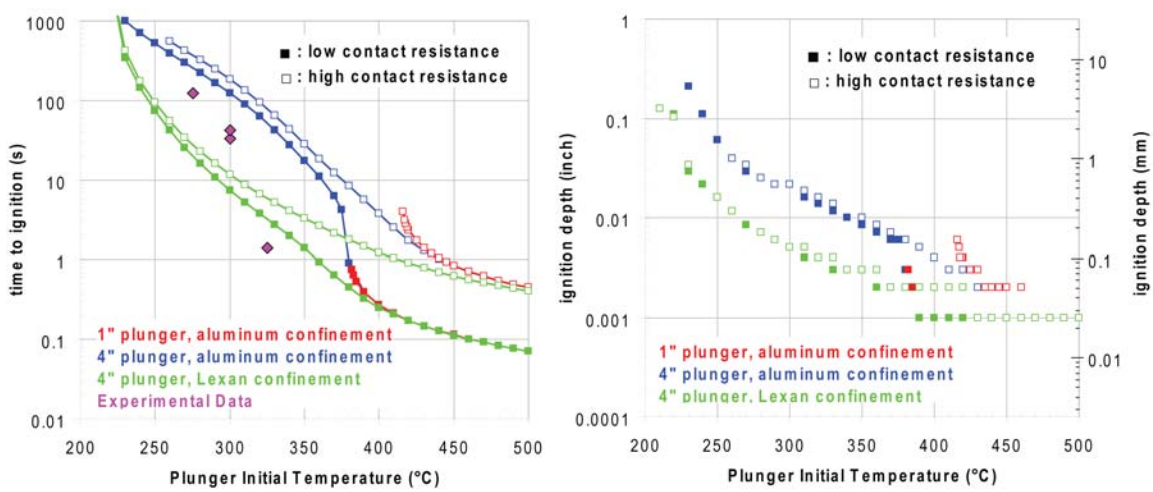

FIG. 9: Time-to-ignition and ignition depth versus plunger initial temperature.

and confinement shim, thermal capacitance of the plunger, and one-dimensionality of the heat flow. The model geometry is shown in Fig. 8 for the case of the 2.54-cm-diameter plunger.

With the baseline design (2.54-cm-diameter plunger) no ignition is predicted for initial temperatures below 380 to 420°C (depending on contact resistance, which ranged from 1.3×10^{-5} to 1.3×10^{-4} m^2-K/W) because the plunger cools off too rapidly. The larger plunger design (10.16-cm-diameter plunger) predicts ignition at much lower temperatures; because of the increased thermal capacitance of the larger plunger, the elevated temperature is maintained for a longer time.

These simulations helped us to recognize that the 2.54-cm-diameter design would be ineffective in much of the temperature range of interest, leading us to the 10.16-cm-diameter design. The simulations also gave us predicted bounding cases through investigating various design parameters, such as the thermal conductivity of the confinement material. A low conductivity material such as Lexan® would lead to noticeably shorter times to ignition than a high conductivity material such as aluminum (the low

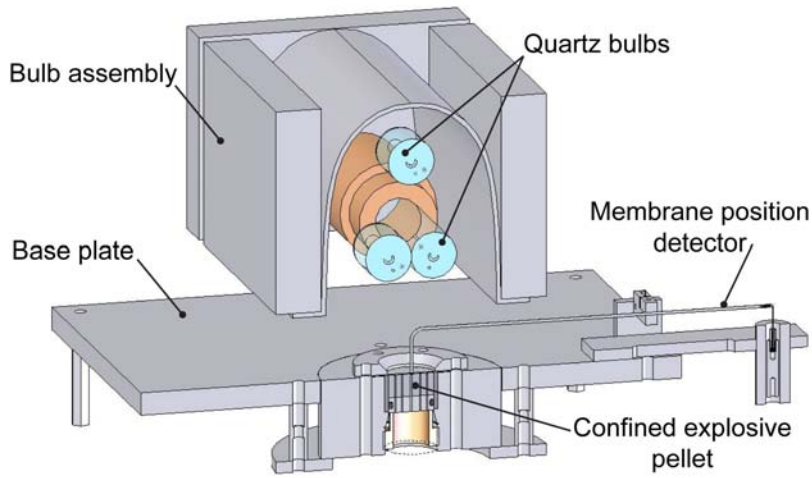

FIG. 10: Illustration of Radiant Heat Test Bed.

conductivity keeps more of the energy within the explosive). As mentioned previously, the experiment ultimately used an insulating PEEK liner in an aluminum casing rather than all Lexan®. The experiments largely fell within the expected low-to-high range of times-to-ignition, with the exception of the highest temperature (325°C) case, though for that case the lower end of the prediction range was only a few seconds different than the experiment.

V. RADIANT-HEAT TEST BED WITH CONFINED EXPLOSIVES

To better represent the real-world hazard of a munition heated in a crosswind pool fire, a radiant-heat test bed has been developed for non-contact heating of a confined explosive pellet. Non-contact heating avoids the challenges observed in the previous sections of a heated plunger with finite thermal mass and potential contact-resistance variations at the plunger-membrane-explosive interfaces.

EXPERIMENT DETAILS

Radiant energy incident on the confined explosive pellet is generated by quartz lamps with tungsten filaments. A cutaway view of the radiant-heat test bed appears in Fig. 10. The test bed consists of the confined explosive pellet, base plate, lamp assembly, and membrane position detector.

The explosive pellet is confined in a vessel that is slightly modified from the vessel used in the PBXN-109 tests of Section III. The major difference in the two vessels is an extended PEEK liner which is flush with the top surface of the explosive pellet. The top clamp ring presses and forms a seal against the PEEK liner instead of relying on an o-ring to form a seal. As before, a 0.020-in-thick aluminum membrane encloses the pellet within the vessel. As a result of non-contact heating and sufficient gas generation at the heated surface (observed in the heated plunger tests) the membrane is expected to bulge due to internal pressurization prior to rupture. A position sensing diagnostic located at the center of the membrane consists of an Invar position rod, pivot, and magnetic position sensor to detect movement of the membrane.

The lamp assembly consists of three 2000-W quartz bulbs of ANSI type BWF. The lamps have an overall length of 19.05 cm (7.5 in) and each bulb has a diameter of 2.54 cm (1 in) with a type CC-8 tungsten filament. Omega phase-delay relays are used to control power to the lamps based on a 0-10 VDC control voltage. At full operation, each bulb requires approximately 16 amps at 120 VAC.

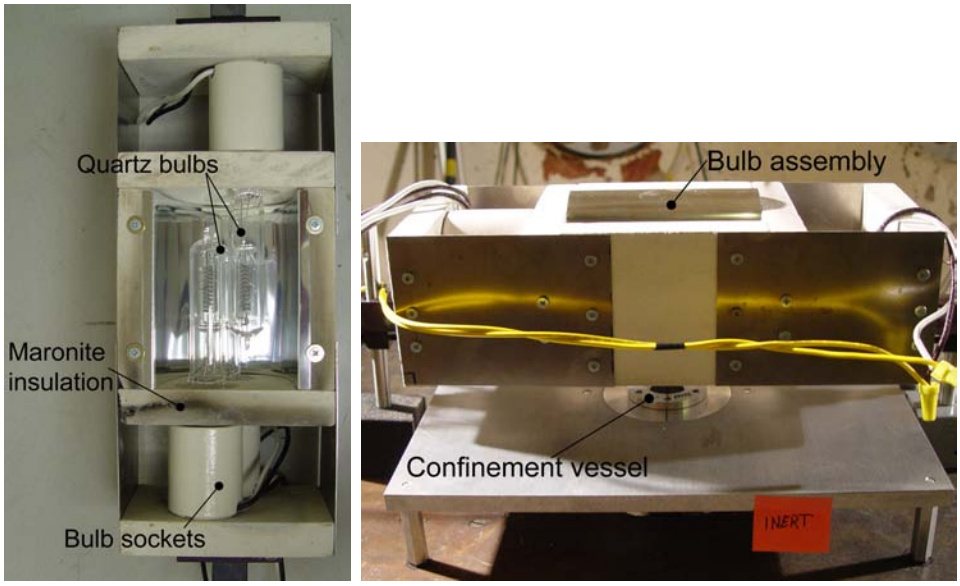

FIG. 11: Photographs of bulb assembly and radiant-heat test bed.

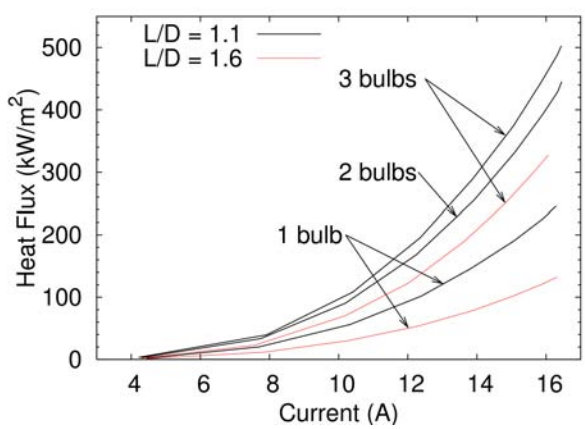

FIG. 12: Incident heat flux from radiant heat test bed.

RESULTS

Incident heat flux measurements were conducted as a function of quantity of bulbs, bulb wattage, location of bulb assembly, and control voltage to the power relay as plotted. The location of the bulb assembly corresponds to the distance, L, between the bulb assembly and the measurement surface which can be normalized by the diameter of the sensing surface, D. Figure 12 plots the incident heat fluxes as a function of supply current for values of L/D equal to 1.1 and 1.6. A Vatell Corporation water-cooled Thermogage Circular Foil Heat Flux Gauge Model TG1000 was used to measure the incident heat fluxes. The emissivity of the gauge surface equals 0.94. The two- and three-bulb lamp assemblies are capable of spanning the desired range of heat fluxes. A maximum value of 500 kW/m^2 was measured.

An initial test was conducted using the radiant-heat test bed to heat an inert pellet of Teflon®. The two-bulb assembly was located at an L/D of 1.1 and the supply current was set to 15.9 A for an incident heat flux of approximately 400 kW/m^2 (Fig. 12). The pellet was instrumented with thermocouples as illustrated in the right side of Fig. 5. The pellet was enclosed within the confinement vessel and a 0.020-in-thick aluminum membrane was installed. The top surface of the membrane had a coating of high temperature paint with emissivity on the order of 0.9. A plot of the measured temperatures appears in

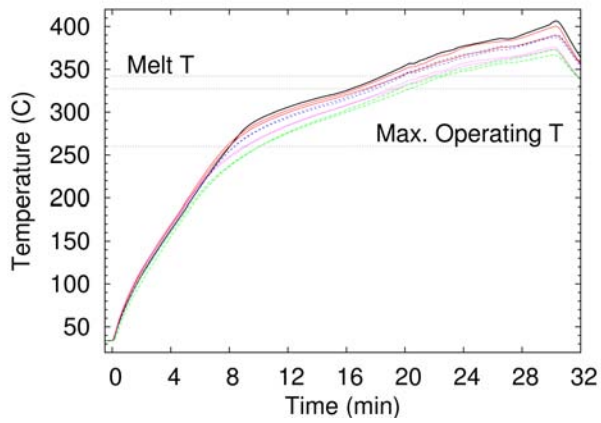

FIG. 13: Plot of Teflon® temperatures using radiant-heat test bed.

Fig. 13. After approximately 8 minutes, the temperatures are ordered based on their location from the center of the pellet and depth from the heated surface. Changes in the measured temperatures correspond to the known maximum operating temperature and upper and lower melting temperatures of Teflon®.

Future work will include continued testing with the radiant-heat test bed using confined pellets of energetic materials. Materials of interest continue to be PBXN-109 and PBX-9501. Thermochemical modeling is anticipated.

VI. CONCLUSIONS

Development of a fast-cookoff test bed has been conducted in terms of both contact and non-contact heating. A heated plunger contacting unconfined and confined pellets of energetic materials demonstrated typical material responses and highlighted the effect of confinement in increasing the violence that ultimately occurs. Thermochemical calculations demonstrated our ability to model the heated-plunger test bed by bounding the measured data with time-to-ignition predictions generated from an entirely aluminum (conductive) or Lexan® (insulative) confinement vessel.

In an effort to simulate the real-world heat fluxes of crosswind pool fires, a radiant-heat test bed was developed. Incident radiant energy generated from high-wattage quartz lamps is incident on the confinement vessel. Initial measurements have demonstrated that the test bed is capable of reaching the incident heat fluxes characteristic of crosswind pool fires. Ongoing experimental and modeling work will use the radiant-heat test bed.

Acknowledgments

We appreciate the many helpful suggestions and discussions that have been facilitated by the Technical Coordination Group (TCG-III) of the Joint DoD/DOE Munitions Program. Mike Oliver at Sandia National Laboratories was instrumental in the development, construction, and testing with the fast cookoff test beds described here. Sandia is a multiprogram laboratory operated by Sandia Corporation, a Lockheed Martin Company, for the United States Department of Energy's National Nuclear Security Administration under Contract DE-AC04-94AL85000.

---

[1] Kaneshige, M. J., Renlund, A. M., Schmitt, R. G., and Erikson, W. W., "Improvements in Cook-Off Models Using Real-Time In Situ Measurement of Temperature and Pressure," *JANNAF 21st Propulsion Systems Hazards Subcommittee Meeting*, Colorado Springs, CO, December 1-5, 2003.

[2] Hobbs, M. L. and Kaneshige, M. J., "Modeling HMX Ignition Using an Enthalpy Formulation," *13th International Detonation Symposium*, Norfolk, VA, July 23-28, 2006.

[3] Hobbs, M. L., Steyskal, M., and Kaneshige, M. J., "Modeling RDX Ignition," *JANNAF 24th Propulsion Systems Hazards Subcommittee*, Newton, MA, May 12-16, 2008.

[4] Kaneshige, M. J., Renlund, A. M., Schmitt, R. G., and Erikson, W. W., "Cook-Off Experiments for Model Validation at Sandia National Laboratories," *12th International Detonation Symposium*, San Diego, CA, August 11-16, 2002.

[5] Dodd, A. B. and Kaneshige, M. J., "Cook-off Model Development and Analysis of Energetic Materials Using Sandia Instrumented Thermal Ignition (SITI) Experimental Data," *13th International Detonation Symposium*, Norfolk, VA, July 23-28, 2006.

[6] Kramer, M. A., Greiner, M., and Koski, J. A., "Radiation Heat Transfer to the Leeward Side of a Massive Object Suspended over a Pool Fire," *International Mechanical Engineering Congress and Exposition*, New York, NY, November 11-16, 2001.

[7] Suo-Anttila, J. M. and Gritzo, L. A., "Thermal Measurements from a Series of Tests with a Large Cylindrical Calorimeter on the Leeward Edge of a JP-8 Pool Fire in Cross-Flow," Tech. Rep. SAND2001-1986, Sandia National Laboratories, Albuquerque, New Mexico, USA, July 2001.

[8] Gritzo, L. A. and Nicolette, V. F., "Coupling of Large Fire Phenomenon with Object Geometry and Object Thermal Response," Tech. Rep. SAND97-1364, Sandia National Laboratories, Albuquerque, New Mexico, USA, 1997.

[9] Gregory, J. J., Jr., R. M., and Keltner, N. R., "Thermal Measurements in a Series of Large Pool Fires," Tech. Rep. SAND85-0196, Sandia National Laboratories, Albuquerque, New Mexico, USA, August 1985.

[10] Erikson, W. W. and Schmitt, R. G., "Modeling Thermal Decomposition and Deflagration in Small- and Munition-Scale Navy Cookoff Experiments," *JANNAF 21st Propulsion Systems Hazards Subcommittee Meeting*, Colorado Springs, CO, December 1-5, 2003.

7 Appendix B

W. W. Erikson, M. A. Cooper and M. S. Oliver, "Radiant Heating Cookoff Experiments and Associated Models", JANNAF 43rd CS, 31st APS and 25th PSHS Joint Meeting, La Jolla, CA. December 2009. Unlimited Release, SAND2009-7192C

Radiant Heating Cookoff Experiments and Associated Models

W. W. Erikson, M. A. Cooper, M. S. Oliver
Sandia National Laboratories*
Albuquerque, NM

ABSTRACT

At Sandia National Laboratories, we have utilized electrically-powered radiant heating devices to represent fire conditions in a controlled, reproducible fashion. The apparatus is used to heat one face of a 2.54 cm diameter cylindrical sample of energetic material which has been confined in a gas-tight structure to mimic a cased munition. Temperatures within the sample near the heated surface are measured using thermocouples. The experiment has evolved over several different designs. Modeling and simulation has been used to understand the heat flow paths though the device. Design modifications were made based on modeling results to help create a situation in which near one-dimensional heat transfer exists through the energetic material pellet.

In this paper, we address the design of the apparatus, models developed to support and interpret the experiments, and results obtained from the tests conducted with energetic materials. A number of experiments have been performed on pellets of the RDX-based explosive PBXN-109. A wide range of fire-like heat fluxes was applied. Simulation-based predictions of time-to-ignition made prior to the experiments represented the experiments well. Ongoing efforts to improve interior temperature measurements are also addressed.

INTRODUCTION

Thermal initiation (cookoff) of energetic material-laden devices such as rocket motors and munitions during accidental fires is an important safety concern. Unfortunately, such fires tend to be highly variable. Fire intensity and the associated thermal loading to a munition changes with location as well as time. Local heat fluxes ranging from 40 - 300 kW/m^2 have been measured within the same fire.[1] It is desirable to develop an experimental apparatus which avoids the variability of fire, but can be adjusted to span the range of heat fluxes expected from fires.

During the past few years we have been developing experiments which will provide controlled, fire-like heat fluxes to energetic material (EM) samples. The first approach with a confined EM sample was to use a heated metal "plunger." In these experiments, a metal cylinder was heated to a known temperature and was then placed in contact with the EM sample. The heated surface of the confinement vessel consisted of a thin metal shim separating the EM from the plunger which provided an initial hermetic seal around the EM.[2]

While the plunger design was able to produce high heat fluxes, the heating profile was not constant. The conduction-driven heat flux dropped substantially over time as the temperature of the EM/shim rose and the plunger cooled. This continuous decrease in applied heat flux is not typical of a fire environment. For an object in a real fire, while there *are* variations with location and flow characteristics, the flux level does not drop nearly so much when the object heats up. This is because the heat transfer in a fire is largely driven by radiant energy exchange between a very hot (typically >1200 K) flame and the object. The T^4 dependency of radiation allows the net radiation flux to the object to remain fairly constant, even though the object might have heated up a couple hundred degrees or more.

The issue with the cooling plunger was partially rectified by increasing the thermal capacitance of the plunger, i.e. making it physically larger. Nevertheless there were still additional concerns with the apparatus: contact resistance between the plunger and the shim played a significant role in the heat transfer to the EM and there were significant lateral energy losses to surrounding parts—multi-dimensional effects became important. Because of these issues, the decision was made to pursue a

Approved for public release; distribution is unlimited.

* Sandia is a multiprogram laboratory operated by Sandia Corporation, a Lockheed Martin Company, for the United States Department of Energy's National Nuclear Security Administration under contract DE-AC04-94AL85000.

different mode of heating—radiant heating lamps. The initial groundwork, described previously in ref. 2, was extended and will be discussed here.

PROCEDURE

The design of the radiant heating apparatus was developed around the following design goals:

- Cylindrical EM samples of 2.54 cm diameter are to be used. One of the flat faces will be exposed to the radiant heat flux.
- Heat fluxes will span the range of 40 to 400 kW/m^2; consistent with a fire environment.
- Temperatures inside the EM itself will be monitored during the tests.
- A hermetic seal will be maintained on the EM sample until after ignition occurs.

Initial Design: Radiant Heating Apparatus #1 (RH-1)

With these goals in mind and building on the preliminary work described earlier,[2] the apparatus was designed and constructed. It was determined that two 2000 W quartz lamps (ANSI Type BWF) could produce the range of heat flux needed. The lamps were held in place within a Marinite® (calcium silicate with inert fillers) box to provide thermal insulation and structural support It can take the high temperatures without smoldering. The lamps were aligned horizontally such that the Tungsten filaments were located directly above the EM within the confinement. The lamp-holding structure was placed on top of an aluminum "floor" into which a large center hole had been cut to allow the introduction of the EM and confining materials. Figure 1 shows the apparatus. On the left is the aluminum floor with the EM confinement inserted. The center 2.54-cm diameter of the aluminum confinement vessel consisted of a 0.05-cm thick aluminum shim coated with Pyromark paint. This shim was attached to the vessel by 6 screws through the confinement ring. On the right is the lamps and lamp support box. An insulating "shutter", also made of Marinite®, located between the bulbs and the test sample allows the bulbs to warm up to the desired power level prior to exposing the lower structure. The shutter is actuated pneumatically.

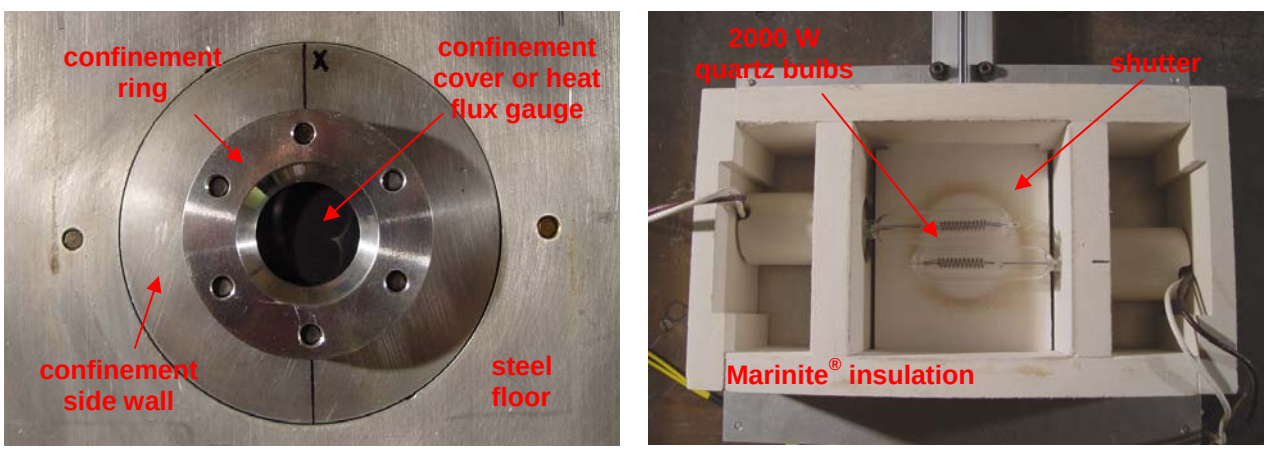

Fig. 1: Pictures of original radiant heating apparatus: Left: EM cover and confinement materials. Right: heating lamps and associated structure.

During scoping tests with the apparatus, a heat flux gauge (Vatell Thermogage circular foil heat transducer) having the same 2.54 diameter size as the EM samples, was placed in the holding fixture. The surface of that gauge was painted with the same surface finish (high emissivity black coating) as the EM sample cover plates would be. Heat flux measurements were made as a function of the current supplied to each lamp. Current was controlled with an Omega "Phase Angle Fired" SCR power controller. This type of controller has a non-linear power delivery response to control settings as shown in Fig. 2 (left). Figure 2 (right) shows the heat flux as measured by the gauge as a function of supplied current. The goal of producing a range of fluxes from 40 to 400 kW/m^2 is within the capability of this apparatus.

The heat flux gauge gives a single reading which averages the response of the entire 2.54 cm diameter sensing surface. However, there was concern that there would be local variations in the heat flux to that surface and that those variations could affect the distribution of the energy delivered to the EM; potentially resulting in hot spots on the EM cover plate. This was particularly of concern for a very thin cover plate which would not distribute the heat well. In order to assess variability of heat flux with spatial location, a modeling approach was used.

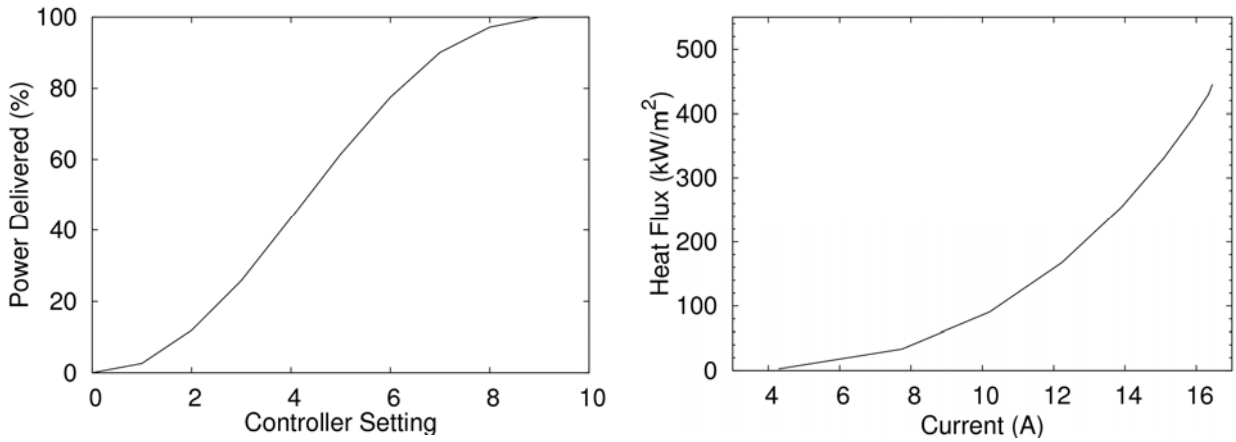

Fig. 2: Behavior of power controller and lamps: Left: Power delivery curve for SCR controller. Right: heat flux delivered to gauge as a function of current delivered to lamps.

There were two goals to the modeling exercise. First, the spatial variation in heat flux was examined as the sensor location itself was moved relative to the lamps (this would help assess the uniformity of the flux distribution within the box itself). Second, we would assess the small-scale variability of the heat flux on the sensor face (or EM cover plate). Finite element models were built and the CALORE heat transfer code.[3] was used to solve the thermal radiation problem. Simulations were performed as the sensor was moved both parallel to and crosswise from the lamp locations. The lamps themselves were modeled as radiating rods in the location of the tungsten filament windings within the actual bulbs. Neither the quartz bulbs nor the holder fixtures were included in the model. However, it was necessary to include the aluminum floor and lamp support box. Figure 3 shows the computational mesh used in this study, from an oblique point of view. Figure 4 shows a top view with the sensor location both centered and moved laterally from the bulb locations.

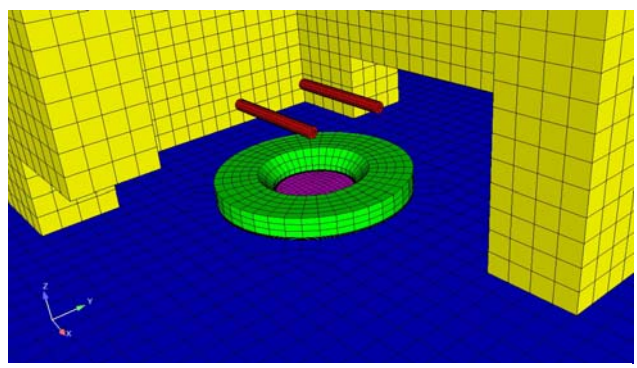

Fig. 3: Finite element mesh used for analysis of the heat flux profile on the sensor locations produced by the radiating bulb filaments. Centered position, oblique view.

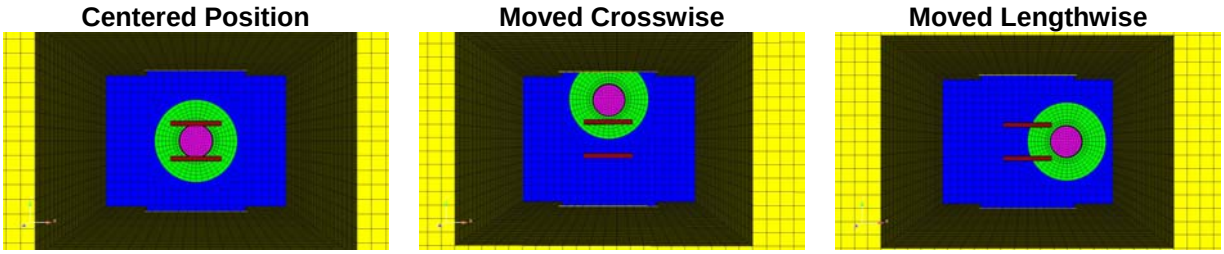

Fig. 4: Top view of finite element mesh showing centered position as well as cases in which the sensor was moved laterally with respect to the bulb filaments.

The first of the two assessments was performed experimentally as well as numerically. That is, the integrated heat flux was determined as the gauge was moved into various locations relative to the radiant heating lamps. In the simulations, the filament radiation temperature was increased until the integrated heat flux across the simulated flux gauge surface was equal to the measured value at the center point. Then that same radiating condition was used for cases where the gauge was moved relative to the bulb filaments and the integrated fluxes were again recorded. Agreement between simulation and experiment was quite reasonable. Spatial variations of the simulated and experimentally measured heat fluxes are shown in Fig. 5 (left side). Agreement was quite good in both crosswise and lengthwise directions with a slightly better level of agreement in the lengthwise direction.

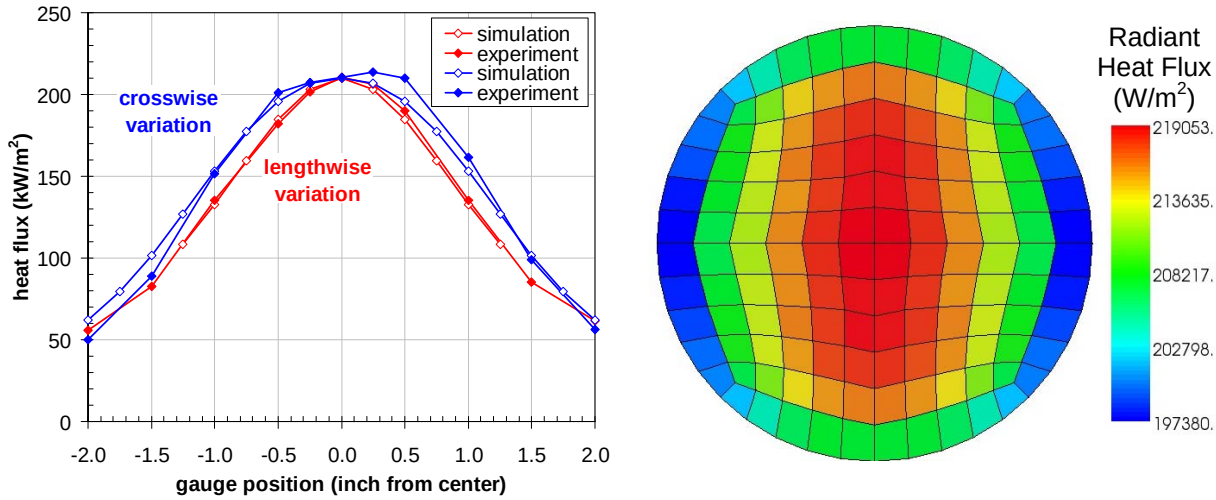

Fig. 5: Left: Experimental and simulation results for integrated heat flux as a function of sensor location relative to bulb filaments. Right: Local heat flux variations over the sensor surface at the centered position from Calore simulations. Maximum to minimum variations are ±11% around the mean. The bulb filaments run in the left-right direction.

The right side of Fig. 5 shows the heat flux distribution predicted by the Calore simulation with the sensor in the centered position. There is about a ±11% maximum variation in heat flux from location to location across the sensor face. The highest heat flux is at the center, as might be expected. The lowest flux levels are at the left and right edges where the surface "sees" less of the bulb filament—part of the field of view is obscured by the confinement ring. (The bulb filaments are aligned in the left-right direction in this image.)

To this point we have established that if care is taken, the model can quite faithfully represent the heat fluxes from the experiments. However, there are two items of concern. First, there seems to be noticeable bulb-to-bulb variation in the experimentally measured heat fluxes. Second, in performing calculations, one would like to be able to reduce the model to a more usable subset; that is, we do not want to have to compute the thermal behavior of the entire structure and supporting equipment in order to simulate the EM response of interest. Rather we would like the apparatus to be sufficiently well-behaved that we can get adequate fidelity by including only the EM and the immediate surrounding materials in the model.

The first concern has been dealt with by a straightforward approach. Rather than simply (but erroneously!) assuming that all bulbs are the same, we characterize each pair of bulbs with the heat flux gauge prior to conducting a live test. That way the flux levels that will be delivered to the EM confining surface will be a known quantity. Generally when a live EM test is conducted, the quartz bulbs are broken and not reusable, so this procedure must be followed for every live shot. The second concern deserves a little more discussion, but we believe that this has been resolved with our latest design. Before describing the most recent design, the behavior of the previous one deserves some discussion as well.

Tests with live EM (the RDX-based explosive PBXN-109) were conducted in the radiant heating apparatus. In those tests, the thin metal shim, which was acting as a confinement cover for the EM, began to deform significantly due to thermal expansion. The center tended to bow upward. In that situation, it became very difficult to determine whether the explosive (which does have a fairly high thermal expansion coefficient, but a very low thermal conductivity) would absorb enough heat and expand sufficiently to maintain contact with the cover plate. We suspect that for several of the tests, the thermal contact between the cover plate and the EM was disrupted, by a gap opening up. Once that happened, it became very difficult to predict the heat transfer to the EM, let alone any chemical reaction behavior induced in the EM.

Design Modifications: Radiant Heating Apparatus #2 (RH-2)

In an attempt to remedy the bowing problem of the cover shim, we made a minor design modification. We added a 6.35 mm thick fused silica window clamped down on top of the shim to provide structural support. The idea was that the window would be transparent to the thermal radiation from the bulb filaments so that the cover plate would still see the very high heat fluxes we wanted to produce. In some respects, this worked, but for most of the tests we did with this design, the glass shattered early in the tests, perhaps from thermal stress. Naturally, a broken window provides little or no structural support and complicates the heat transfer to the cover plate. As a result, the fused silica window design was abandoned. Examples of the behavior of two of these tests are shown in Figure 6.

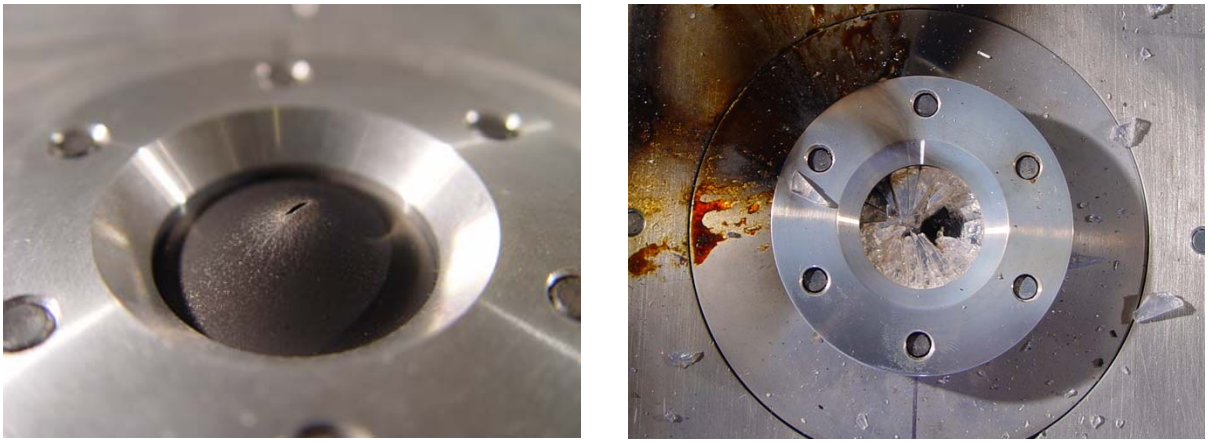

Fig. 6: Aftermath of two radiant heating tests with PBXN-109. Left: Using apparatus design RH-1. In this test, the cover plate bowed upward and eventually a small leak formed in the top center. Right: Using apparatus design RH-2. A fused silica window placed on top of the cover plate shattered.

Even if the covers had not deformed and the windows not shattered, the heat transfer behavior of that design was still complicated. Simulations showed significant multidimensional heat conduction from the shim to adjacent confinement materials such as the cover ring and side wall, resulting in the EM near the upper corners being heated both from the upper face and the side or radial direction face. Attempts to isolate the cover shim were made by including a PEEK liner and layers of Kapton to minimize metal-to-metal contact. Even so, considerable multidimensional effects remained. This resulted fundamentally because the conduction path through the metal side housing was highly preferred instead of the low-conductivity EM—and heat flows in the path of least resistance. As a result, it was very difficult to determine how much of the radiant energy incident on the surface of the cover plate actually arrived at the EM. Furthermore, measurements of the cover plate temperature were not really feasible either by thermocouples (mounting difficulties and interference with apparatus) or by optical sensors (signal would be swamped by reflected light from lamps). Hence this design yielded a very difficult boundary condition for data correlation or modeling (would require modeling the whole apparatus).

Current Design: Radiant Heating Apparatus #3 (RH-3)

The most recent design is one in which all three of these issues (the cover plate deformation, the multidimensional heat transfer effects, and the unknown boundary conditions) are addressed. Changes to the baseline included replacing the all aluminum housing with a two-piece, PEEK (Quadrant EPP Ketron® PEEK 1000) and aluminum housing and replacing the thin cover plate and the confinement ring with a 6.35 mm thick, 7.62-cm-diameter aluminum cover plate. The confinement was designed to provide a hermetic seal. A ring-shaped knife edge is machined into the cover plate. As the bolts are tightened, the knife edge digs into the upper surface of the PEEK to provide a gas-tight seal on the upper face. Below the EM an o-ring prevents gas leakage outside the support piston. The thermocouple probes, which pass through the piston, also have a gas-tight fit; they are sealed with epoxy bonded to the bottom of the piston support. Figure 7 shows the current design of the EM confinement portion of the apparatus.

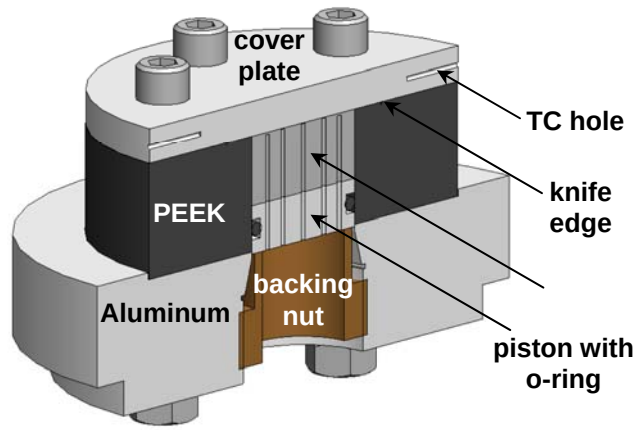

Fig. 7: Current design of confinement for EM (RH-3).

Simulations were made to predict the behavior of the design using finite element models (see Fig. 8). The simulations showed that there was nearly one-dimensional heat transfer in the vertical direction. The improvements happened for a couple reasons. First, since the aluminum has high thermal conductivity, the thick cover plate is able to smooth out variations in temperature resulting from uneven radiant heating (c.f. the right side of Fig. 5). Second, since PEEK and the EM are both fairly good insulators, there was no preferential path for heat conduction either to the outside (i.e. through the PEEK) or to the inside (through the EM). The combination of these two effects resulted in a nearly one-dimensional (vertical direction) flow of energy through the EM. There were concerns that the six steel bolts which hold the apparatus together would be preferential heat conduction paths and produce complex temperature profiles. To analyze their effects, the bolts were included in the finite element model. Though there are some multi-dimensional effects associated with the bolts, the simulations indicated that heat transfer along them did not adversely affect the profile within the EM itself.

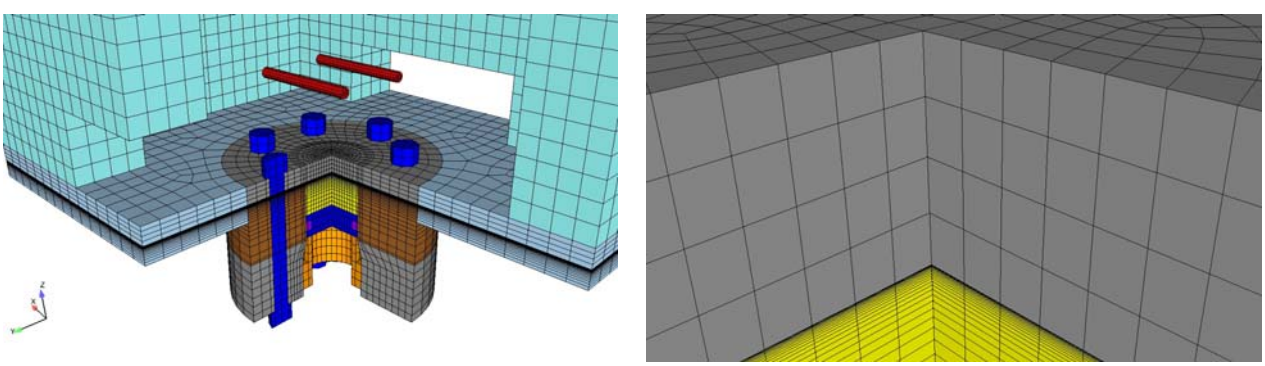

Fig. 8: Cutaway of the finite element mesh of the current apparatus design (RH-3). Left: full model with lamp filaments, box and confinement materials. Right: Detail emphasizing interface between aluminum cover plate and EM—a very fine mesh was used to capture the steep temperature gradient occurring just under the EM surface. The finest mesh gradation was 13 μm.

In practice, including the thick aluminum cover plate solved the other two issues as well. The added structural strength of the plate eliminated the thermally-induced bowing deformation seen with the thin cover plate. The thickness also made it possible for the plate to be instrumented with thermocouples.

Holes were drilled laterally in the plate to permit the insertion of two thermocouple probes. As a result, the temperature boundary condition on the upper surface of the EM could be measured directly (temperature gradients through the high-conductivity aluminum are small).

Live EM Experiments

Tests were conducted with each of the three versions of the radiant heat apparatus. Early in the development process, tests were conducted with Teflon®, Delrin®, or Vespel® as EM surrogate materials. Live EM experiments used the RDX-based explosive PBXN-109. For apparatus RH-1 (thin shim cover, no window) only one live EM shot was conducted. Six experiments were conducted with apparatus RH-2 (thin shim cover, fused silica window) and four experiments were conducted with apparatus RH-3 (thick cover plate, 2-part PEEK/aluminum housing). Table I lists the experimental conditions for each of these live EM shots. (Numbering begins with FCO-47, the first radiant heating test with live EM. Lower and omitted numbers were for tests with the plunger-type apparatus, or were radiant heating tests with inert samples).

Table I: Radiant Heating Experiments with Live EM (PBXN-109)

SNL Test Number	Device Type	Incident Heat Flux (kW/m^2)	Time to Rupture (sec)	Ignition Temp. (°C)*	Time to Ignition (sec)	Notes
FCO-47	RH-1	390 ±11.9	231	154	239	no shutter used, shim ruptured, rapid venting
FCO-50	RH-2	277	12	123	none	no shutter used, shim bulged, ruptured window, test stopped before lamps reached full power
FCO-51	RH-2	294 ±2	13	122	13	shutter with 30 sec. warmup, shim bulged, ruptured window
FCO-52	RH-2	156 ±11	28	141	28	shutter with 30 sec. warmup, shim bulged, ruptured window
FCO-53	RH-2	48 ±1	1889	169	none	shutter with 3 min. warmup, window broke, No EM ignition
FCO-54	RH-2	72 ±16	302	181	302	shutter with 2 min. warmup, window did NOT break, vent/rupture out side below shim
FCO-55	RH-2	102 ±9	69	167	69	shutter with 30 sec. warmup, window did NOT break, vent/rupture out side below shim
FCO-56	RH-3	79 ±1	158	163	158	shutter with 2 min. warmup, venting at cover plate-PEEK interface
FCO-57	RH-3	51 ±1	371	187	371	shutter with 2 min. warmup, venting at cover plate-PEEK interface
FCO-58	RH-3	149 ±1	71.2	165.5	71.2	shutter with 2 min. warmup, o-ring not installed in piston, venting at cover plate-PEEK interface
FCO-59	RH-3	296 ±3	28.5	147.7	28.5	shutter with 2 min. warmup, venting at cover plate-PEEK interface

* ignition temperature as measured by the nearest internal thermocouple.

Simulations

Finite element models were developed for the RH-2 and RH-3 designs. For RH-2 a two-dimensional, axisymmetric model was used; a representation of the model is shown in Fig. 9,. That figure shows an approach to isolate the EM thermally and to eliminate metal-to-metal conduction paths by using a PEEK cylinder sleeve as well as strategically placed Kapton tape, and a similar approach was attempted in the actual device. The thermal path modification plans did work to some extent. However, the housing acted as a very large heat sink and much of the incident radiant energy was transferred there via various lateral conduction paths. There was clearly not one-dimensional behavior. Though, when care was taken to represent the important details of the geometry, reasonable agreement between models and experiments could be achieved. A graded mesh density was given in the vertical direction in the EM with very fine (13 μm) resolution near the EM-shim interface. This was done to capture the strong gradients that would result in the poorly conducting EM subject to a large heat flux and to be able to determine fairly accurately at what depth the model predicted ignition runaway would occur. A one-dimensional model was also built, which assumed that all the energy incident on the surface shim was transferred to the EM. Comparison with data was poor for the one-dimensional model of RH-2.

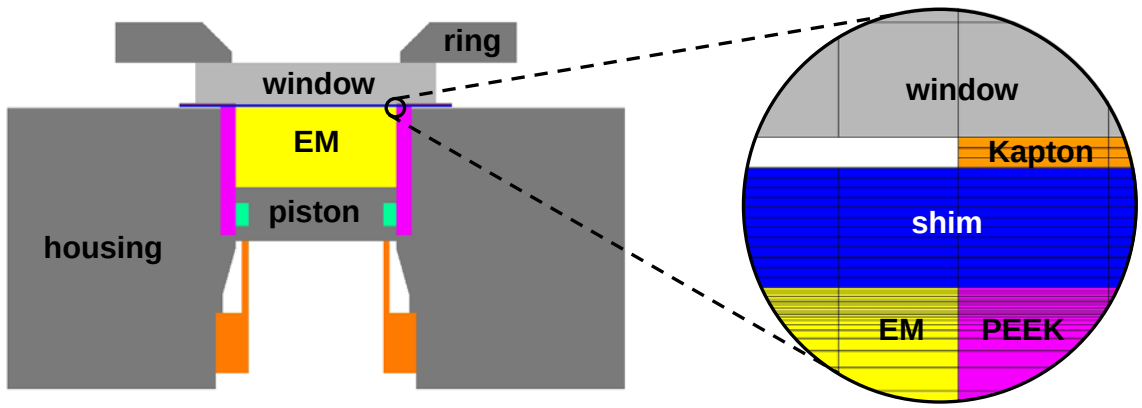

Fig. 9: Finite element representation of design RH-2. This model was treated as 2-D axisymmetric.

For the RH-3 design, since we had already used a full 3-D model in designing the apparatus, the same 3-D model was used to predict the thermal behavior (see Fig. 8). A one-dimensional model was also used. This model was different than the 1-D model of RH-2; here it included three layers: a 6.35 mm thick aluminum layer, a 12.7 mm thick EM layer, and an 8.64 mm thick layer representing the support piston. The mesh spacing was 1 µm in the region near the aluminum-EM interface.

One of the purposes of the fast cookoff test was to determine whether the reaction mechanism obtained from slower heating tests applies at the faster heating rates. To test this, we used thermophysical properties and a decomposition reaction mechanism for PBXN-109 developed from a previous joint Navy-DOE program on slow cookoff.[4] All of the thermal finite element models were solved numerically using the CALORE code.

RESULTS

Thermal Behavior

For the 1-D and 2-D models of the RH-2 apparatus, a constant heat flux boundary condition was applied on the upper shim location. Each simulation was allowed to proceed until a thermal runaway state was achieved somewhere within the EM, at which point the simulations halted. The time to reach the runaway state was recorded as was the location (i.e. depth) within the EM of the runaway state. Figure 10 shows the simulated response in terms of time to ignition (left) and ignition depth (right) as a function of applied heat flux. Also shown on the time to ignition graph are the data points for the experimental data taken with the RH-2 apparatus. Note that the 2-D model does seem to capture most of the trends in the time to ignition data, with about a 2.5 decades-per-decade slope. The 1-D model showed reaction happening much faster than it actually did and with a slope of 1.43 decades-per-decade. Lateral heat losses to the housing and other material—represented by the 2-D model but not captured in the 1-D model—clearly made a difference.

The ignition depth chart (Fig. 10 right side) indicates some level of mesh coarseness is slightly affecting the results—causing a stair-step result in a couple of places. The thermal runaway point was seeking to be established somewhere between node points. (Note that this mesh was already quite refined—with 13 µm grid spacing at the EM-shim interface and gradually increasing further into the EM.) Since the code forces the runaway to happen at a node, it “snapped to” the nearest node. A more refined mesh would be expected to yield smoother results. The dashed lines on the chart indicates the depths of the thermocouples in the experiment. The model predicts that in order to capture the thermal runaway at all, flux levels at the low end of the 40-400 kW/m^2 range are necessary. Higher flux levels produce ignition depths so close to the surface that it may be difficult to capture the transient thermal response. (The

predicted ignition depth is on the order of a few tens to a few hundreds of μm!) These results suggest that a different way of installing thermocouples might be warranted in order to capture the desired transients. Note that we have not reported the experimental thermocouple responses here. We have been largely unable to capture the thermal ignition runaway from the thermocouple traces in the tests conducted to date. An exception was for one test at a low flux level (FCO-56 test using RH-3 apparatus) in which the center TC started to show signs of a thermal excursion prior to ignition. Also note that the one-dimensional model predicts approximately a one half decade-per-decade slope in ignition depth as a function of incident heat flux; the 2-D model has a much steeper slope. From the results here, it is clear that the one-dimensional model is not acceptable.

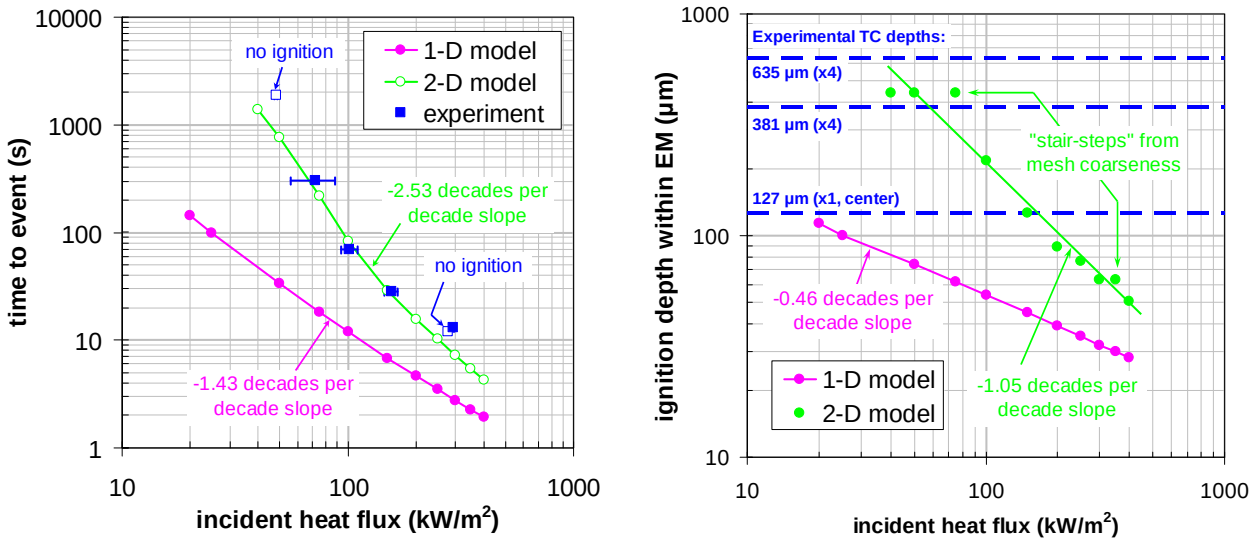

Fig. 10: Results from experiments and simulations of the radiant heat apparatus with the window (RH-2). Left: time to ignition as a function of incident heat flux (note two shots did not ignite the EM, but did rupture the confinement). Right: ignition depth with the EM as a function of incident heat flux.

Figure 11 shows the results from the 1-D and 3-D models of RH-3, with the left showing the time to ignition and the right side showing the ignition depth, each as a function of incident heat flux. It is worth mentioning that the time-to-ignition curve using the 3-D model was produced prior to the experiments being conducted—it was a true prediction. The 1-D model results were obtained later. Note that the ignition time vs. incident flux graph shows that both models show essentially the same slope (around 1.3 to 1.4 decades per decade), but that there is a noticeable offset between the two.

The explanation for the offset is that the heat flux input (the x-coordinate of the graph) was determined differently for the two models. For the 1-D model, the full value of heat flux is simply imposed on the upper surface of the 6.35 mm thick plate. However, in the 3-D model, a temperature assigned to the bulb filaments was the actual imposed boundary condition; the filaments then radiated to the object surfaces with a non-uniform spatial distribution. For comparison with experiment, the heat flux applied to the 1-D model was inferred based on an average flux over the center circle of 2.54 cm diameter (the same area as would be covered by the heat flux gauge). But the radiant heat flux drops off noticeably away from the center location (c.f. Figs. 5 and 12). Hence while the center 2.54 cm circle was receiving the full gauge-value heat flux as shown in Fig. 12 (left), the rest of the 7.62 cm circle received far less radiant energy (Fig. 12 right). On average, the heat flux received on the full aluminum plate (including the contribution from the bolts) is only 65% of the average which hits the center 2.54 cm circle.

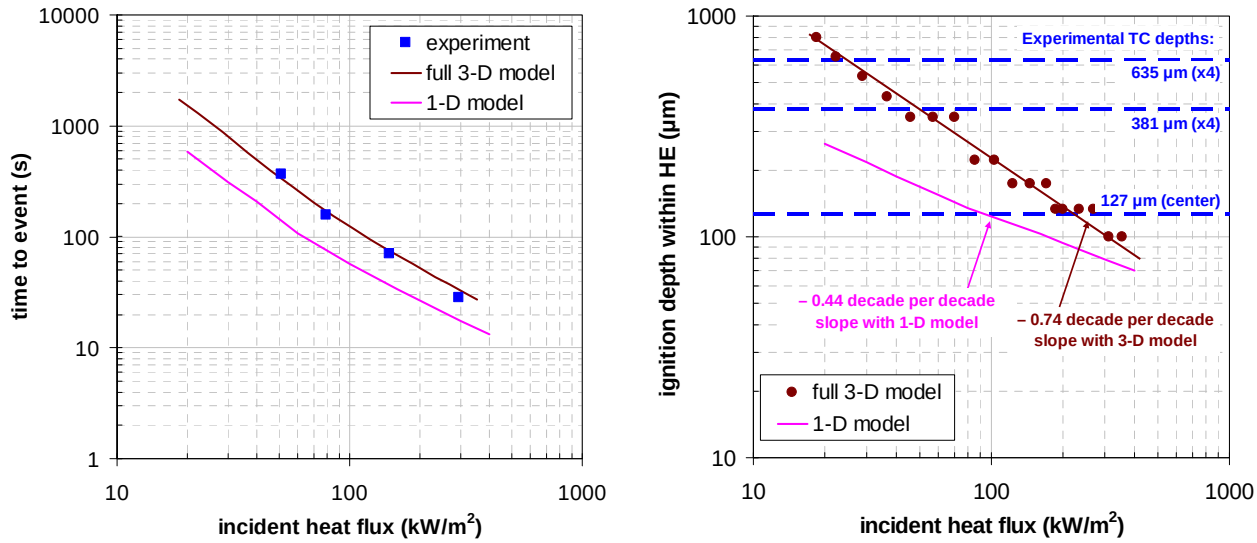

Fig. 11: RH-3 design results showing experimental results and corresponding 3-D and 1-D model results as a function of incident heat flux. Left: time to ignition, Right: depth of ignition.

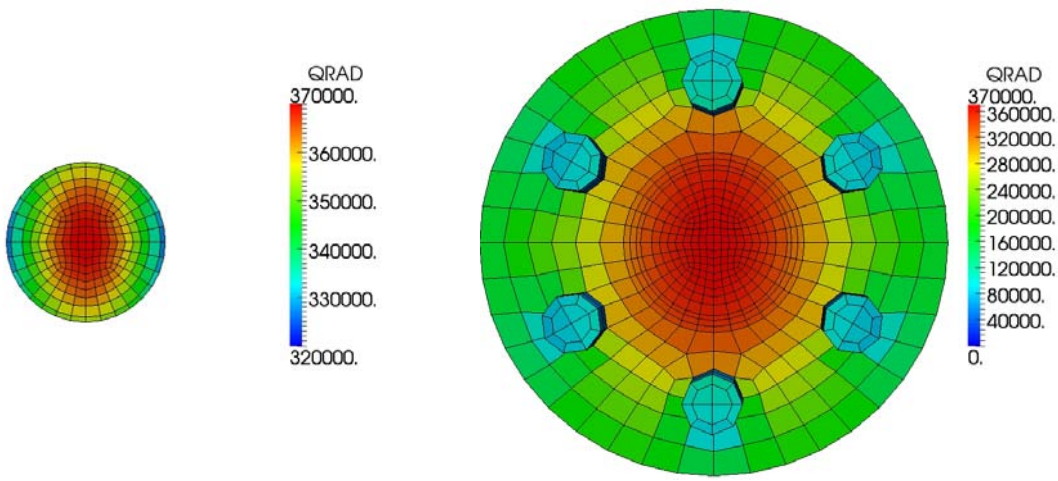

Fig. 12: Heat flux distribution predicted by 3-D model. Left: Center 2.54 cm diameter circle. Right: full 7.62 cm diameter circle associated with the aluminum cover plate.

In addition to the average heat flux reduction resulting from the uneven distribution as described above, there are also energy losses down the bolts which result in a reduced effective heat flux at the EM location. Fortunately, we can estimate the magnitude of these losses. This was done by using readings from the thermocouples embedded in the aluminum plate as boundary conditions to two inverse heat conduction problems. The first inverse problem assumes that conduction is through three layers (i.e. cover plate, EM, piston); the second inverse problem assumes that conduction is through a single layer (i.e. steel bolts). Time-temperature readings from the thermocouples were used to determine the surface heat fluxes for each of the two inverse problems using the IHCP1D code.[5] These are shown in Fig. 13 where the left side graph shows the heat flux that would be conducted through the EM and the right side graph shows the heat flux that would be conducted down the bolts (if, as we have assumed, the upper end of the bolts follows the temperature history outlined by the thermocouple traces.) Notice that the flux level through the bolts is considerably higher than through the EM. (For that matter, the flux level through the bolts is even higher than the flux level imparted by the lamps to the surface. This is possible because the aluminum plate acts as a collector and funnels energy preferentially to the bolts.)

By using the results shown in Fig. 13 along with the cross sectional area of the six bolts relative to the area of EM and PEEK, the fraction of the incident energy which is "lost" to the bolts can be estimated. It works out to be a value from 10 to 20%, as shown in Fig. 14. The flux applied to the 1-D model can then be adjusted to reflect the amount by dividing by 0.65 (from the uneven distribution from the lamps) and also dividing by 0.8 to 0.9 (from fraction of energy *not* conducted down the bolts). This effectively shifts the flux to a higher value, making it correspond with what would be seen by the heat flux gauge in the center 2.54 cm diameter circle. Figure 15 shows that shifted result for the 1-D model. Two lines are shown, one corresponding to the range of 10% bolt heat loss and the other to the 20% bolt loss. In shifting to the gauge-corresponding heat flux, the 1-D model result also aligns with the experimental time-to-ignition data.

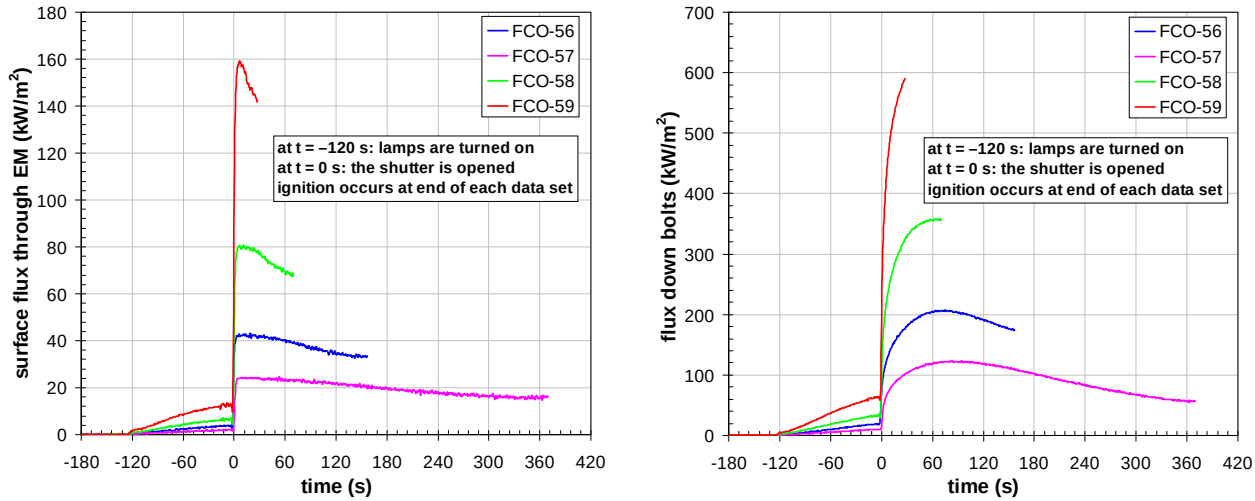

Fig. 13: Heat fluxes through the EM (left chart) and through the bolts (right chart), based on inverse calculations using cover plate thermocouple data as a boundary condition to the IHCP1D code.[5]

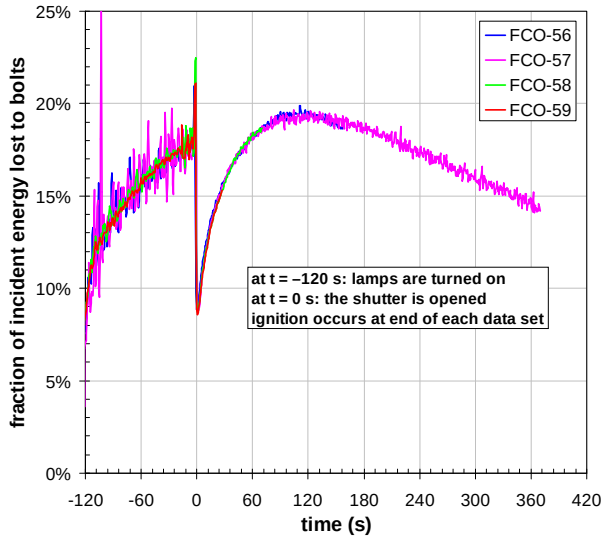

Fig. 14: Fraction of energy incident on upper surface conducted down through the bolts in the RH-3 tests.

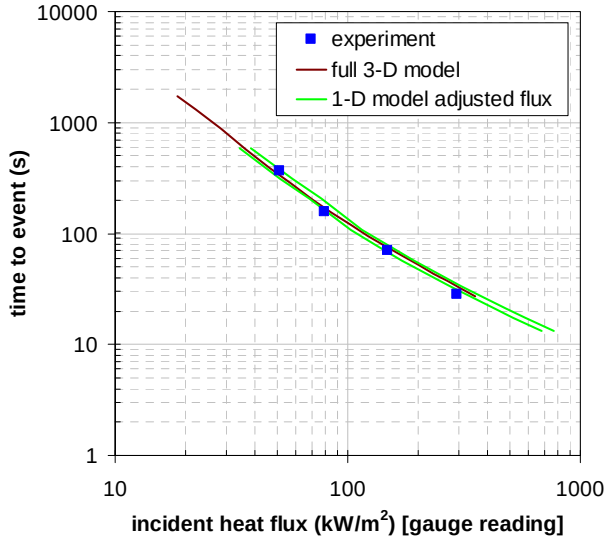

Fig. 15: Time to ignition for RH-3 design tests, showing experimental data, and the full 3-D and the adjusted 1-D model.

Incidentally, Fig. 13 also shows that there is some heat flux "leakage" through the shutter prior to its withdrawal at time zero. The 6.35 mm thick Marinite® shutter was apparently not quite sufficient to block all the radiant energy during the two-minute heat up. It may be possible to improve the performance of the apparatus by either increasing the thickness of the insulating shutter or by adding a thin reflective layer (e.g. shiny aluminum) to the upper surface of the shutter. Either of these would tend to reduce the heat transfer through the shutter to the device.

Mechanical Behavior

With the RH-1 and RH-2 designs, it is difficult to make any definitive conclusions about the mechanical behavior of the apparatus. It is clear that thermal expansion of the cover shim played a role (e.g. in contributing to the bowing as shown in Fig. 6, left) as did the fused silica window. However, contributions from thermal decomposition, gas generation, and the associated pressurization also affected the observed deformation pattern. It is not certain that sufficient information is available to allocate the contributions of the various phenomena that occurred sufficient to model it. For instance, the temperature of the shim is unknown, so it would be difficult to estimate the thermal expansion.

In contrast, the RH-3 design does appear to have behaved in a sufficiently predictable fashion to reasonably attempt to model its behavior. For instance, the pattern of dark streaks on the underside of the cover plate departing radially from the center core seems to indicate a fairly uniform flow of combustion products once the confinement was breached (see Fig. 16). Moreover, the aluminum cover plate seems to have plastically strained during the cook-off event in a fairly regular manner (see Fig. 17). Deflections were measured from the deformed plate using a Scan Shark V4 model 32640-1 contour probe (Hexagon Metrology, Inc.) mounted on a 2.8 m Infinite model 25526-09 seven-axis manipulator arm (Romer, Inc.) The zero deflection location defined as the ring around the bolt holes. The measurements exhibit six-fold symmetry, following the bolt pattern. The maximum deflection for the FCO-57 test was 2.66 mm at the center of the cover plate.

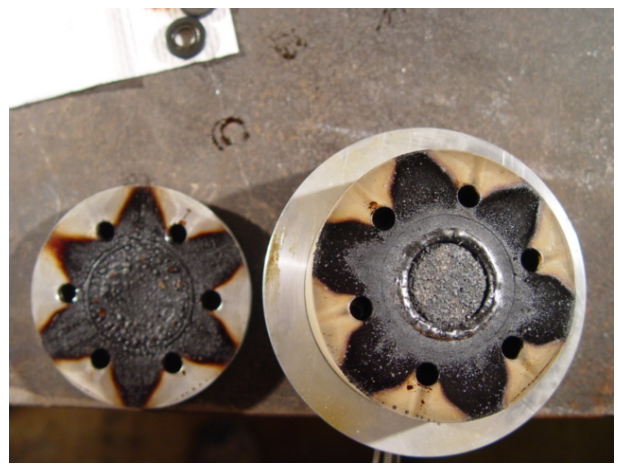

Fig. 16: Pattern of combustion products on the disassembled apparatus from FCO-56. On the left is the underside of the cover plate; on the right is the PEEK confinement with the EM residue in the center.

The fact that the cover plate was plastically strained, and did not fully recover its original shape, can also be used to develop a model of what happened during the experiment. A quarter-symmetric finite element model of just the confinement apparatus (i.e. without the complications associated with the lamps, support plate, and insulation box) was built to look at mechanical deformations caused by quasi-static pressure loads. In that model, the EM was removed. In its place, a pressure boundary condition was applied at interior surfaces. The cover plate was disconnected mechanically from the PEEK; only the bolts were holding it down. The ADAGIO[6] quasi-static solid mechanics code was used to solve for the material stresses, strains and deformations. Calculations were performed for a range of internal pressures from 0 to 138 MPa (0 to 20,000 psi).

Figure 18 shows the computational mesh and the equivalent plastic strain in the aluminum cover plate as a function of internal pressure. Note that the deformation pattern looks qualitatively like that observed experimentally in Fig. 17, with the peak at the center of the plate as expected. The model indicates that 2.66 mm deflection at the upper surface would occur at a pressure of about 128 MPa (18,600 psi). Since the quasi-static assumption employed in the model does not account for the additional material strength associated with inertia, the actual peak internal pressure achieved in the experiments may have been even higher, presuming, of course, that the mechanical properties [moduli, yield strength, etc.] used in the

model were reasonable estimates. Note that the cover plate material was at elevated temperature at the time of the deformation; we have not considered temperature-dependent properties here.

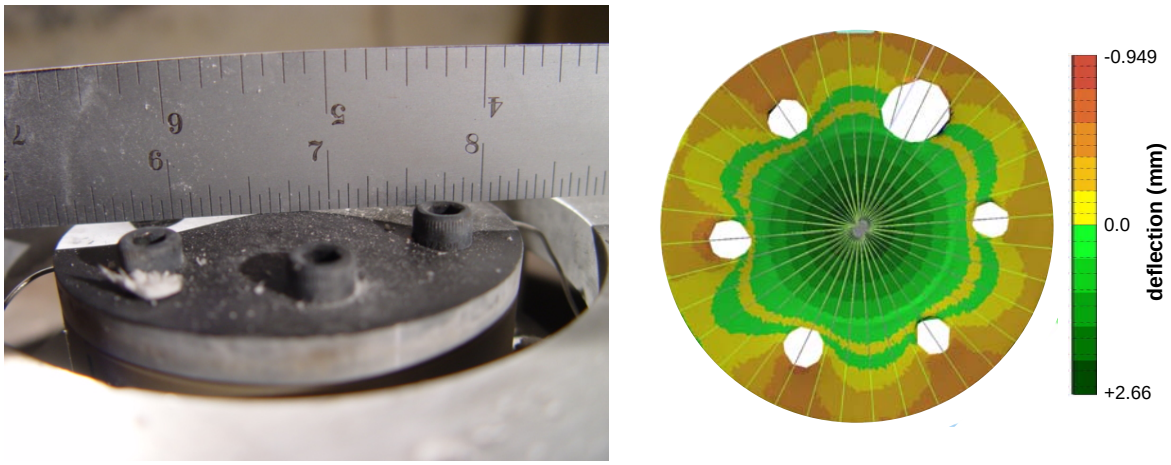

Fig. 17: Deformed cover plate from test FCO-57. Left: photograph of post-test unit. Right: measured deflection profiles. Peak deflection is 2.66 mm at the center.

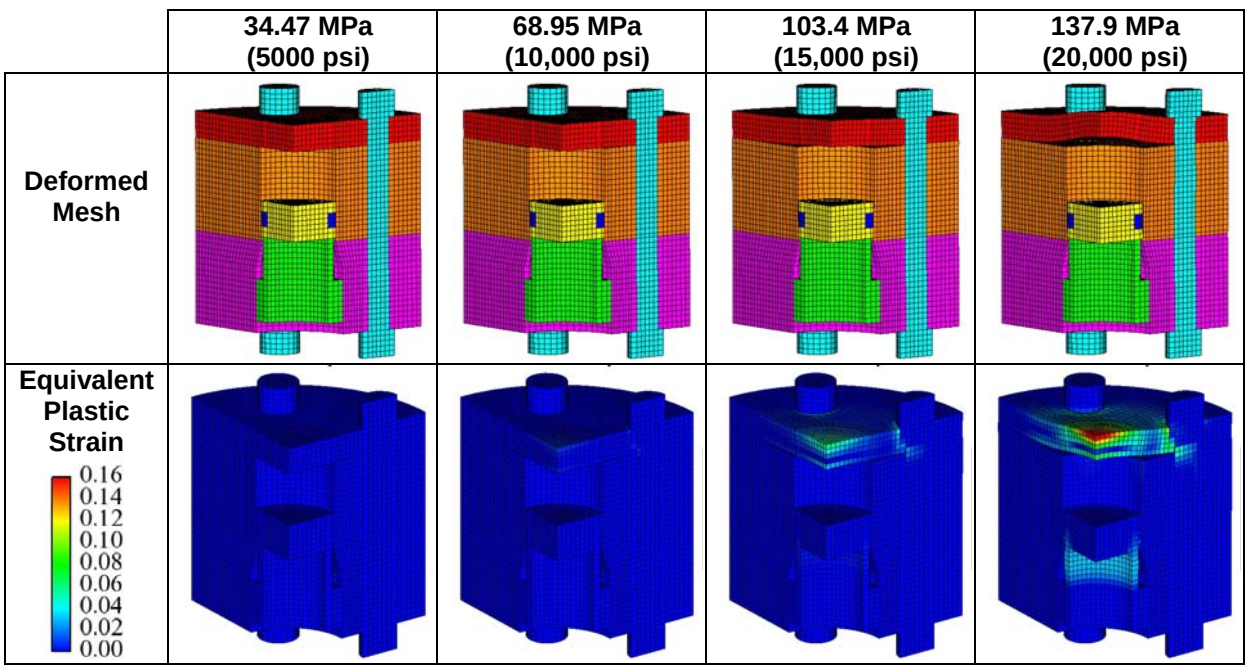

Fig. 18: Finite element model of mechanical deformation of device induced by internal pressure loading. Upper set of images shows the deformed mesh, the lower set shows the equivalent plastic strain. Pressure loading increases from left to right in each set.

CONCLUSIONS

Three different versions of radiant heating cookoff experiments were developed during the evolution of the current project. RH-1 used a thin shim as a cover; RH-2 added a transparent window; and RH-3 changed to a thick aluminum cover plate with a two-part PEEK and metal housing. Two quartz lamps were used to provide the energy input to the apparatus. A shutter was used to allow the lamps to warm up to operating conditions prior to suddenly exposing the device to the radiant heating. The apparatus

was characterized using heat flux gauges. Live EM tests were conducted with each of these versions, yielding data on time to ignition as a function of incident heat flux. The RH-3 design is believed to be the best of the three. It appears to give nearly one dimensional heat flow and has the added benefit of a thermocouple to serve as a boundary condition.

Finite element models of the various experimental setups were created. Thermal models were able to capture the spatial heat flux distribution produced by the radiant heating lamps. The models were also able to represent well the time to ignition for PBXN-109. For the RH-1 and RH-2 apparatus, there were sufficient lateral heat transfer losses that a 2-D model was required; a 1-D model could not capture the trends. For the RH-3 apparatus, 3-D modeling results were true predictions, performed prior to the experiments being conducted and captured well the time to ignition. RH-3 could also be modeled with a 1-D model, but it was necessary to make some corrections to the imposed heat flux to account for non-uniformities and bolt heat losses which had been represented in the 3-D model.

Mechanical deformations of the thick cover plate of RH-3 were. Computations using finite element models operating under quasi-static pressure loading were also performed. Qualitative agreement with the deformation shape was achieved using the model, and estimates were made as to the peak internal pressure loading achieved during the experiment.

FUTURE PLANS AND RECOMMENDATIONS

While substantial progress has been made in developing a radiant heating fast cookoff apparatus, there are still areas for improvement. As of yet, we have not been able to capture the thermal runaway using our thermocouples, mounted within the EM. These K-type thermocouples have a sheath diameter of 0.08 cm and are positioned within holes drilled into the EM. As shown previously, ignition depth varies with incident heat flux and so thermocouple placement must be varied as a function of test conditions. Efforts are underway to develop a thermocouple probe with multiple temperature-sensing junctions evenly spaced along a single probe. Development of this probe is being pursued in-house by manual construction with fine thermocouples on a Kapton film and through printing of metal nanoparticle slurries directly onto a Kapton substrate.

Other areas for improvement include eliminating the thermal leakage through the shutter during warm up. A reflective aluminum sheet placed atop the shutter may help in this regard.

ACKNOWLEDGEMENTS

We appreciate the efforts of John Liwski who made the deformation measurements. We gratefully acknowledge the funding and support provided from the DoD/DOE Joint Munitions Program under Technical Coordination Group-III, managed by Gene Hertel and Mike Kaneshige.

REFERENCES

[1] J. M. Suo-Anttila and L. A. Gritzo, “Thermal Measurements from a Series of Tests with a Large Cylindrical Calorimeter on the Leeward Edge of a JP-8 Pool Fire in Cross-Flow,” SAND 2001-1986, Sandia National Laboratories Report, July 2001.

[2] M. A. Cooper, W. W. Erikson, D. Sandoval, and M. J. Kaneshige, “Development of a Fast-Cookoff Test Bed at Sandia National Laboratories,” *JANNAF JPM / CS / APS / EPTS / PSHS Joint Meeting*, Boston, MA, May 2008.

[3] Calore Development Team, "Calore A Computational Heat Transfer Program", Vol. 2 User Reference Manual for version 4.6, SAND 2008-0098P, Sandia National Laboratories, June, 2008.

[4] M. J. Kaneshige, A. M. Renlund, R. G. Schmitt and W. W. Erikson, “Cook-off Experiments for Model Validation at Sandia National Laboratories, Twelfth International Detonation Symposium, p.821, San Diego, CA, August, 2002.

[5] J. V. Beck, "User's Manual for IHCP1D: Program for Calculating Surface Flux from Transient Temperatures inside Solids," Beck Engineering Consultants, Co. Okemos, MI, 1999.

[6] SIERRA Solid Mechanics Team, “Adagio 4.11 User’s Guide” SAND2009-3215, Sandia National Laboratories, May 2009.

8 Appendix C

Engineering drawings of the major components of the confinement vessel: Cover Plate, Upper and Lower Casing, Pedestal and Pellet Support.

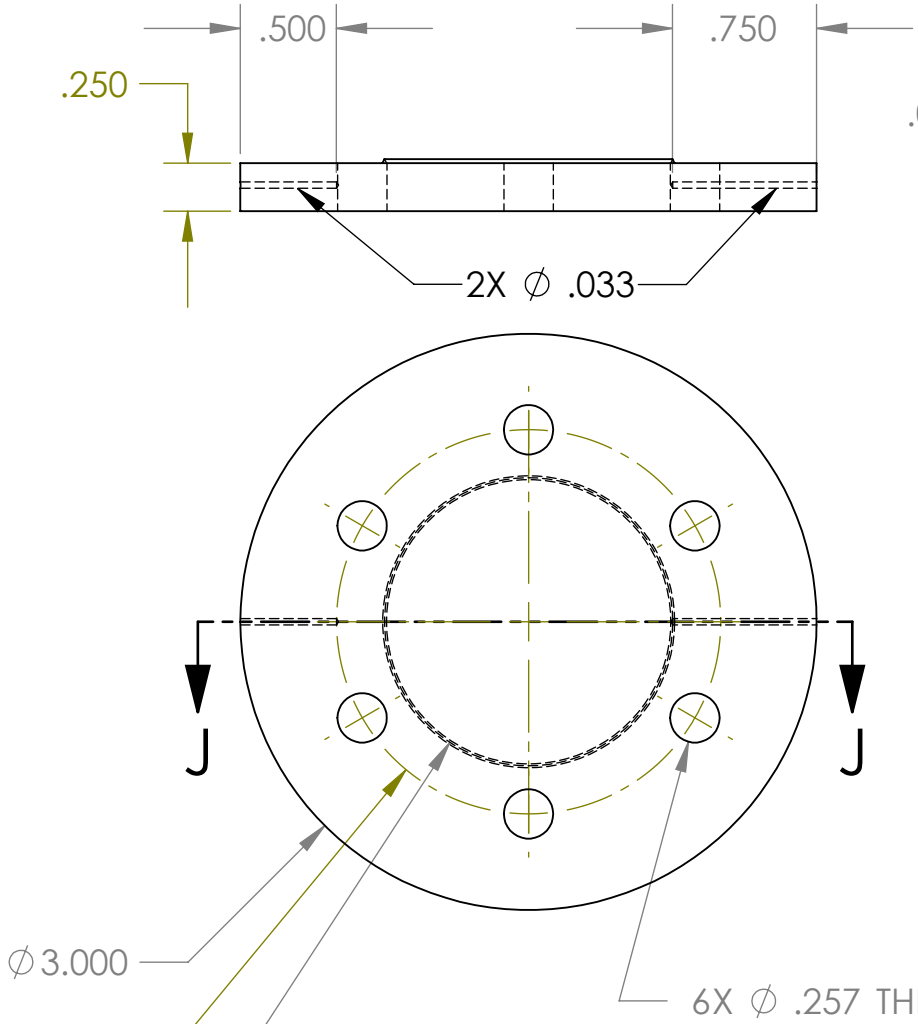

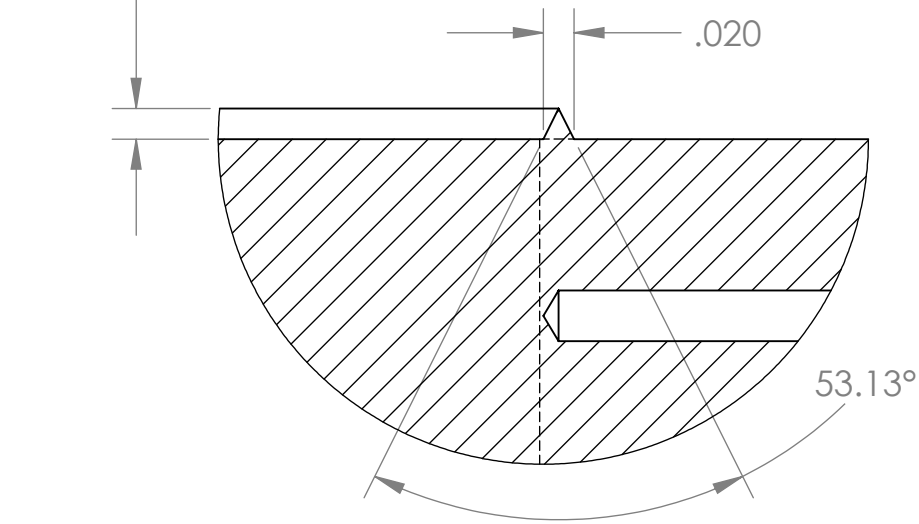

DETAIL K
SCALE 8 : 1

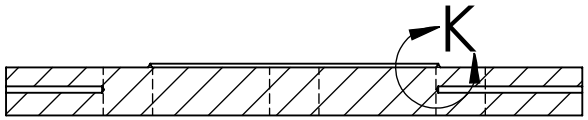

SECTION J-J

PROPRIETARY AND CONFIDENTIAL

THE INFORMATION CONTAINED IN THIS DRAWING IS THE SOLE PROPERTY OF SANDIA NATIONAL LABS. ANY REPRODUCTION IN PART OR AS A WHOLE WITHOUT THE WRITTEN PERMISSION OF SANDIA NATIONAL LABS ISPROHIBITED.

NEXT ASSY	USED ON
APPLICATION	

UNLESS OTHERWISE SPECIFIED:

DIMENSIONS ARE IN INCHES
TOLERANCES:
FRACTIONAL ±
ANGULAR: MACH ± BEND ±
TWO PLACE DECIMAL ±.01
THREE PLACE DECIMAL ±.005

INTERPRET GEOMETRIC TOLERANCING PER:

MATERIAL 6061 T6 Aluminum

FINISH 32

DO NOT SCALE DRAWING

	NAME	DATE
DRAWN		
CHECKED		
ENG APPR.		
MFG APPR.		
Q.A.		

COMMENTS:

Radient Heated Pellet Assembly

TITLE:
Cover Plate

SIZE	DWG. NO.	REV
A		

SCALE: 1:1 WEIGHT: SHEET 2 OF 10

5 4 3 2 1

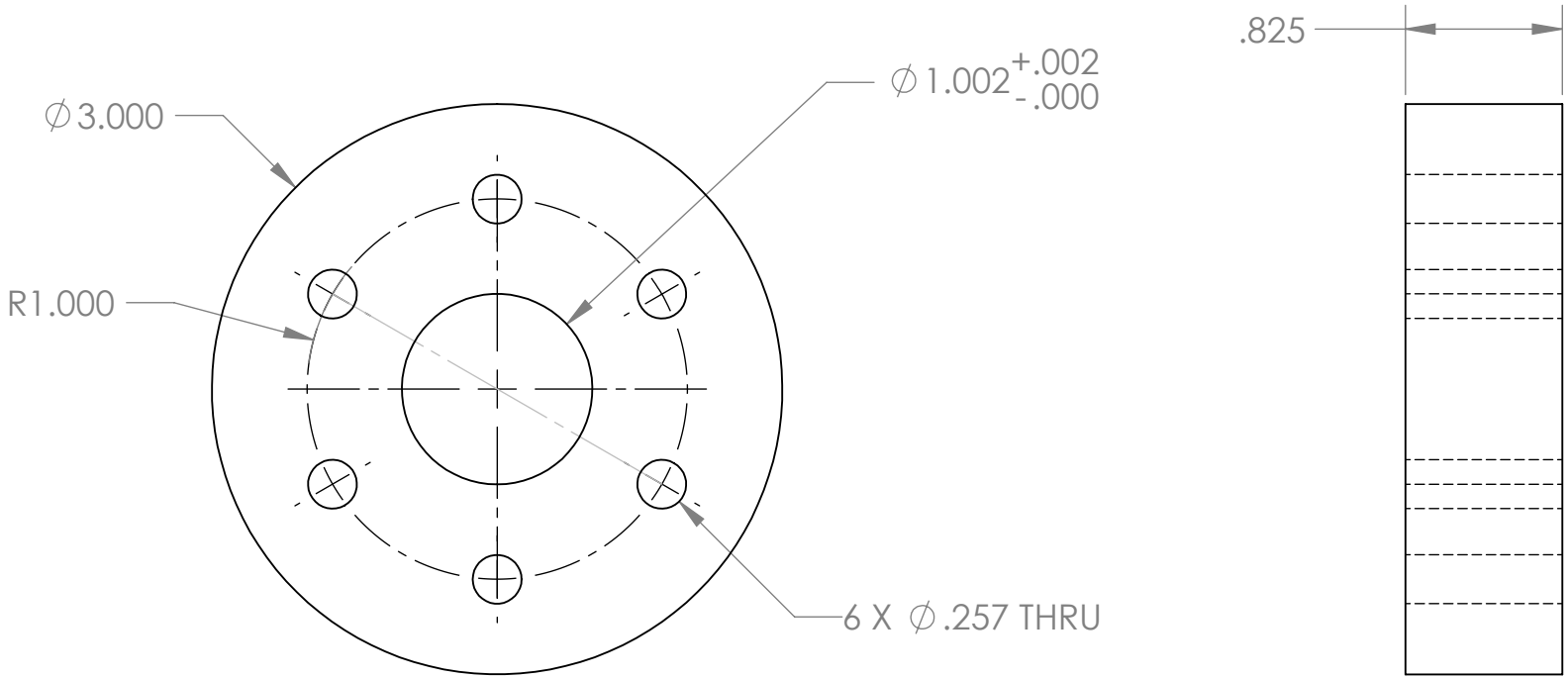

PROPRIETARY AND CONFIDENTIAL

THE INFORMATION CONTAINED IN THIS DRAWING IS THE SOLE PROPERTY OF SANDIA NATIONAL LABS. ANY REPRODUCTION IN PART OR AS A WHOLE WITHOUT THE WRITTEN PERMISSION OF SANDIA NATIONAL LABS ISPROHIBITED.

NEXT ASSY	USED ON
APPLICATION	

UNLESS OTHERWISE SPECIFIED:

DIMENSIONS ARE IN INCHES
TOLERANCES:
FRACTIONAL ±
ANGULAR: MACH ± BEND ±
TWO PLACE DECIMAL ±.01
THREE PLACE DECIMAL ±.005

INTERPRET GEOMETRIC TOLERANCING PER:

MATERIAL
Glass filled PEEK

FINISH

DO NOT SCALE DRAWING

	NAME	DATE
DRAWN		
CHECKED		
ENG APPR.		
MFG APPR.		
Q.A.		

COMMENTS:

Radiant Heated Pellet Assembly

TITLE:
Upper Casing

SIZE	DWG. NO.	REV
A		

SCALE: 1:1 | WEIGHT: | SHEET 3 OF 10

5 4 3 2 1

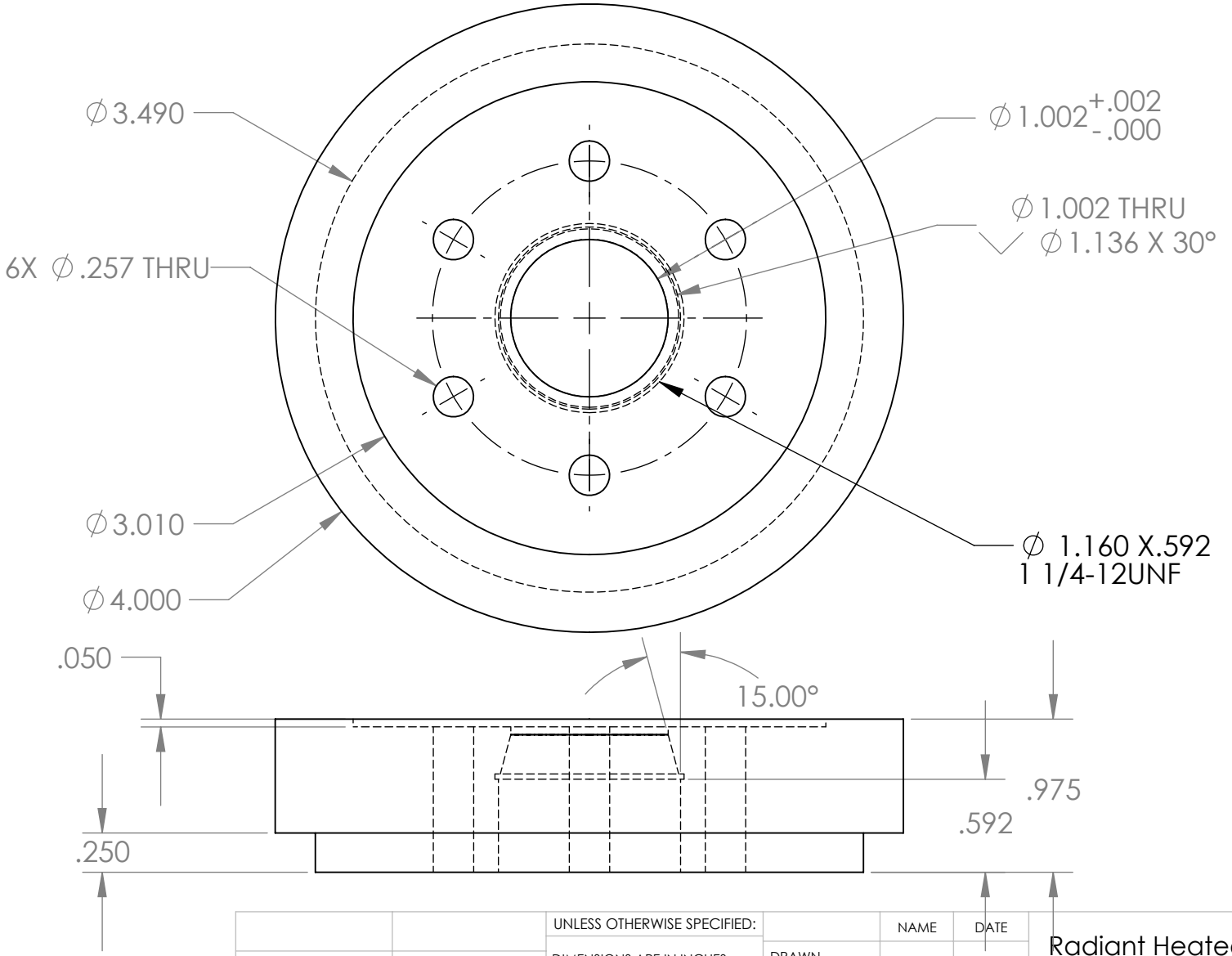

		UNLESS OTHERWISE SPECIFIED:		NAME	DATE
		DIMENSIONS ARE IN INCHES TOLERANCES: FRACTIONAL ± ANGULAR: MACH ± BEND ± TWO PLACE DECIMAL ± THREE PLACE DECIMAL ±	DRAWN		
			CHECKED		
			ENG APPR.		
			MFG APPR.		
		INTERPRET GEOMETRIC TOLERANCING PER:	Q.A.		
		MATERIAL 6061 T6 Aluminum	COMMENTS:		
NEXT ASSY	USED ON	FINISH			
APPLICATION		DO NOT SCALE DRAWING			

Radiant Heated Pellet Assembly

TITLE:

Lower Casing

SIZE	DWG. NO.	REV
A		
SCALE: 1:2	WEIGHT:	SHEET 4 OF 10

PROPRIETARY AND CONFIDENTIAL

THE INFORMATION CONTAINED IN THIS DRAWING IS THE SOLE PROPERTY OF SANDIA NATIONAL LABS. ANY REPRODUCTION IN PART OR AS A WHOLE WITHOUT THE WRITTEN PERMISSION OF SANDIA NATIONAL LABS ISPROHIBITED.

5 4 3 2 1

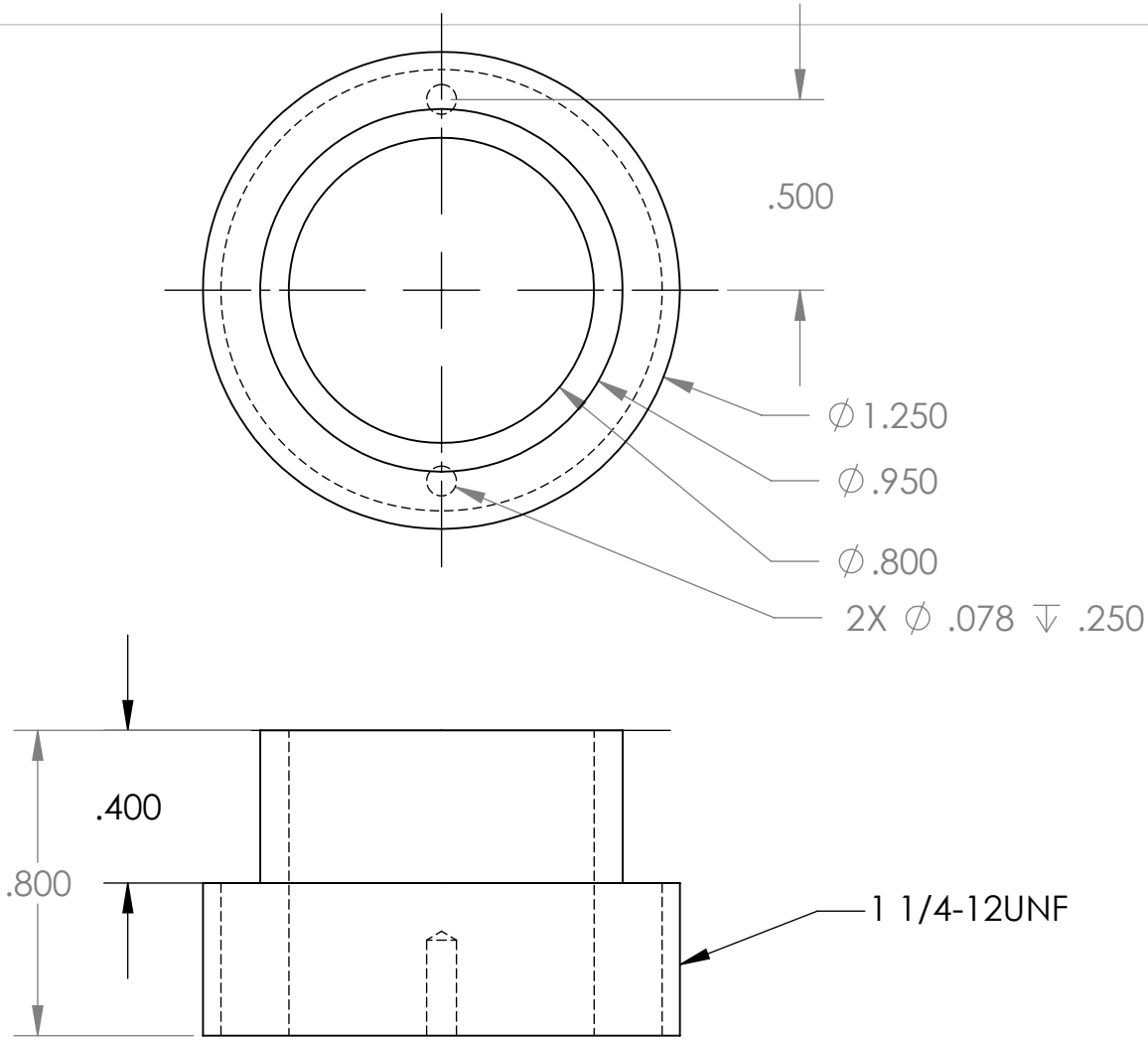

PROPRIETARY AND CONFIDENTIAL

THE INFORMATION CONTAINED IN THIS DRAWING IS THE SOLE PROPERTY OF SANDIA NATIONAL LABS. ANY REPRODUCTION IN PART OR AS A WHOLE WITHOUT THE WRITTEN PERMISSION OF SANDIA NATIONAL LABS ISPROHIBITED.

NEXT ASSY	USED ON
APPLICATION	

UNLESS OTHERWISE SPECIFIED:

DIMENSIONS ARE IN INCHES
TOLERANCES:
FRACTIONAL ±
ANGULAR: MACH ± BEND ±
TWO PLACE DECIMAL ±
THREE PLACE DECIMAL ±

INTERPRET GEOMETRIC TOLERANCING PER:

MATERIAL
Brass

FINISH 32

DO NOT SCALE DRAWING

	NAME	DATE
DRAWN		
CHECKED		
ENG APPR.		
MFG APPR.		
Q.A.		

COMMENTS:

Radient Heated Pellet Assembly

TITLE:
Pedestal

SIZE	DWG. NO.	REV
A		

SCALE: 1:1 | WEIGHT: | SHEET 8 OF 10

5 4 3 2 1

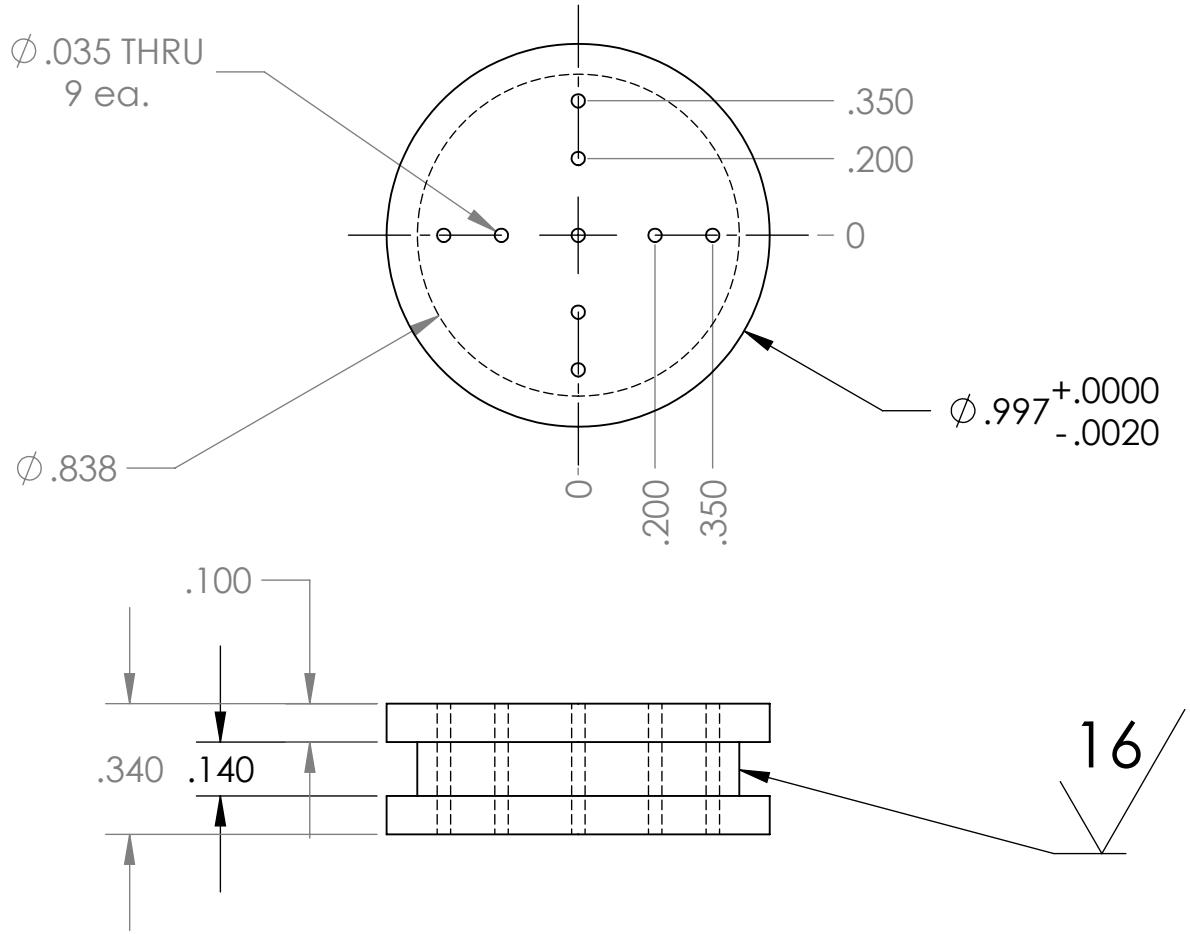

		UNLESS OTHERWISE SPECIFIED:		NAME	DATE
		DIMENSIONS ARE IN INCHES TOLERANCES: FRACTIONAL ± ANGULAR: MACH ± BEND ± TWO PLACE DECIMAL ±.01 THREE PLACE DECIMAL ±.005	DRAWN		
			CHECKED		
			ENG APPR.		
			MFG APPR.		
		INTERPRET GEOMETRIC TOLERANCING PER:	Q.A.		
		MATERIAL 6061 T6 Aluminum	COMMENTS:		
NEXT ASSY	USED ON	FINISH 32			
APPLICATION		DO NOT SCALE DRAWING			

Radient Heated Pellet Assembly

TITLE:
Pellet Support

SIZE	DWG. NO.	REV
A		
SCALE: 2:1	WEIGHT:	SHEET 9 OF 10

PROPRIETARY AND CONFIDENTIAL

THE INFORMATION CONTAINED IN THIS DRAWING IS THE SOLE PROPERTY OF SANDIA NATIONAL LABS. ANY REPRODUCTION IN PART OR AS A WHOLE WITHOUT THE WRITTEN PERMISSION OF SANDIA NATIONAL LABS ISPROHIBITED.

5 4 3 2 1

DISTRIBUTION:

1	MS 0836	W. W. Erikson, 01516
1	MS 0836	A. S. Geller, 01516
1	MS 0836	M. L. Hobbs, 01516
1	MS 1192	D. Sandoval, 01678
1	MS 1453	J. L. Moya, 02550
1	MS 1454	M. A. Cooper, 02554
1	MS 1454	M. J. Kaneshige, 02554
1	MS 1454	L. M. G. Minier, 02554
1	MS 0899	Technical Library, 9536 (electronic copy)

Sandia National Laboratories